Heterogeneous REE+Y distribution in Early Paleozoic shelly phosphorites: implications for enrichment mechanisms

Kaarel Lumiste[1,2]*, Liisa Lang[1], Päärn Paiste[1], Aivo Lepland[1,3,4], Kalle Kirsimäe[1],

[1]Department of Geology, University of Tartu, Ravila 14A, 50411 Tartu, Estonia

[2]Geological Survey of Estonia, F. R. Kreutzwaldi 5 44314, Rakvere, Estonia

[3] CAGE – Centre for Arctic Gas Hydrate, Environment and Climate, Department of Geosciences, UiT The Arctic University of Norway, 9037 Tromsø, Norway

[4]Geological Survey of Norway, 7491 Trondheim, Norway

*Corresponding author: email kaarel.lumiste@ut.ee

Abstract

Sedimentary phosphorites are important carriers of Rare Earth Elements and Yttrium (REE+Y). Primary biogenic and sedimentary apatite contain very low amounts of REE+Y and enrichment of these elements occurs during diagenesis. Although the influence of post-depositional processes on REE+Y concentrations in sedimentary phosphorites is well established, the processes controlling the degree of enrichment are poorly constrained. In this study, we examine the REE+Y composition of Early Paleozoic shelly phosphorites of the Baltica paleocontinent, using ICP-MS and LA-ICP-MS. Phosphate containing phases in these deposits are (i) phosphatic brachiopod shells, (ii) phosphatic clasts and (iii) phosphatic grain coatings. Measured REE+Y concentrations range from 162.7 to 2415.3 mg/kg. The distribution of REE+Y in phosphatic shells and clasts is heterogeneous, with the highest concentrations found in the outer margins. In the phosphatic shells, remnants of skeletal apatite contain higher REE+Y concentrations than authigenic apatite in baculate laminae. In addition, our results show significant locality-based variability, with up to 14 times differences in REE+Y concentrations from localities situated only a few tens of km apart. Based on (i) the distribution of REE+Y in apatite, (ii) La_N/Yb_N and La_N/Sm_N ratios pointing to diagenetic REE+Y uptake from sediment pore-fluids, as well as (iii) variable pyrite content, the geographic variations of REE+Y in sedimentary phosphorites of the Baltica paleocontinent are most parsimoniously explained by differences in local redox conditions during early diagenesis.

1. Introduction

Rare Earth Elements (REE) are group of 15 elements from La to Lu with similar chemical properties. REE are often grouped together with Yttrium (referred to collectively as REE+Y) due to identical valence and similar ionic radii of Y and Ho. Under oxygenated redox conditions, most of the REE+Y are in a trivalent state, and their geochemical behaviour is extraordinarily coherent. However, slight changes in the stability of inorganic REE complexes, stemming from the gradual filling of the 4f orbital, lead to increased stability of heavy REE (HREE, Ho to Lu) in seawater (de Baar et al., 1991), resulting in around an order of a magnitude higher Post Archean Australian Shale (PAAS, Taylor and McLennan, 1985) normalized concentrations of dissolved HREE compered to light REE (LREE; La to Nd) in the water column (de Baar et al., 2018). Also, the REE+Y with empty and half-filled 4f orbitals (La and Gd, respectively) are anomalously enriched in seawater (Bau, 1999; Masuda and Ikeuchi, 1979). The largest variability in marine REE+Y concentrations is related, however, to the behaviour of Y, Ho and redox-sensitive Ce. Under oxic conditions, Ce^{3+} is oxidized to Ce^{4+} (McArthur and Walsh, 1984) and is preferentially scavenged by sinking Fe-Mn oxyhydroxide particles, leaving oxic seawater depleted in Ce (Byrne and Sholkovitz, 1996). The Fe-Mn oxyhydroxides also preferentially scavenge Ho over Y, leading to Y enrichments expressed in Y/Ho ratios of >50 in seawater, compared to chondritic value of around 28 (Bau and Dulski, 1996; Minami et al., 1998). As a result, modern marine PAAS normalized REE+Y patterns display weak La and Gd enrichments (Bau, 1999), strong Ce depletion, HREE enrichment (de Baar et al., 1985), and Y/Ho ratios of >52 (Nozaki et al., 1997).

Sedimentary apatite (Ca-phosphate) and phosphate rocks in general are prominent sinks for the REE+Y in marine settings and are a potential source for the world's growing REE demand (Emsbo et al., 2015). Phosphate phases in sediments can be broadly divided into two groups: (i) biogenic apatite composed of skeletal remnants of apatite-secreting animals, such as brachiopods (e.g., Heinsalu et al., 1994; Lécuyer et al., 2004) vertebrates, and coprolites (e.g., Garnit et al., 2017; Lécuyer et al., 2004); and (ii) microbially mediated authigenic sedimentary apatite (Arning et al., 2009b; Compton and Bergh, 2016; Föllmi, 1996). Both biogenic and sedimentary apatite incorporate low amounts of REE+Y during their formation (Lécuyer et al., 1998; Lumiste et al., 2019). As REE+Y are taken up quantitatively after deposition (Reynard et al., 1999), the REE-Y composition of primary sedimentary and/or biogenic apatite contain information regarding the seawater composition and prevailing

paleoredox conditions during their formation (e.g., Emsbo et al., 2015; Felitsyn et al., 1998; Lécuyer et al., 2004, 1998; Reynard et al., 1999; Shields and Webb, 2004; Sturesson et al., 2005; Wright et al., 1987; Zhao et al., 2013). For example, preserved marine REE+Y signatures can be (with some limitations) inferred even from apatite found in metamorphosed Archean rocks (Birski et al., 2019; Lepland et al., 2002). However, due the susceptibility of apatite to accumulate a variety of trace metals and especially REE+Y (Pan and Fleet, 2002), the primary signatures are easily muted by prompt uptake of REE+Y during apatite recrystallization on relatively short timescales already in early diagenetic conditions (Auer et al., 2017; Lumiste et al., 2019; Shields and Stille, 2001).

Cambrian - Ordovician boundary beds in the Baltic Paleobasin in northern Estonia are composed of shallow marine peritidal to beach zone sandstones with abundant phosphatic bioclasts of lingulate brachiopods (Heinsalu and Viira, 1997; Puura, 1996) that form the largest un-mined phosphorite reserve in the European Union with an estimated total resource of about 800 million tons of P_2O_5 (Raudsep, 1997, 1987). Earlier studies of Estonian shelly phosphorite have documented significant variability of REE+Y concentrations (Baturin and Ilyin, 2013; Felitsyn et al., 1998; Lécuyer et al., 1998; Sturesson et al., 2005) but the causes of this variability have remained unclear. In this contribution, we study the REE+Y composition and distribution in phosphatic shells and phosphatic pebbles/clasts in Cambrian-Ordovician phosphorites of Estonia aiming at deciphering the REE+Y uptake and redistribution mechanisms in these sediments.

2. Geological setting

Shelly phosphorites in Estonia and north-western Russia were deposited during Cambrian-Ordovician transition in a shallow epicontinental sea of the Baltica paleocontinent (Heinsalu and Viira, 1997). Furongian-Tremadocian phosphorite of the Kallavere Formation is made up of yellow to light grey cross-bedded quartz sandstones with abundant phosphatic bioclasts and occasional carbonaceous mudstone interbeds (Sturesson et al., 2005), with a maximum thickness of up to 17 m (Heinsalu and Viira, 1997). The main apatite-containing particles in the Kallavere Formation are lingulate brachiopods, dominantly represented by *Ungula ingrica* species (Heinsalu et al., 1994; Puura, 1996). Brachiopod valves occur as intact shells or fragments of varying sizes, forming lenses and coquinas throughout the formation.

Shells contain abundant diagenetic pyrite and hematite (Lang et al., 2016), giving them a distinct black-grey or reddish colour, respectively. In addition to biogenic apatite, the medium- to coarse-grained sandstone of the Kallavere Formation contains reworked phosphatic clasts similar to what is found in the phosphorite beds of Vassbo, Sweden (Wallin, 1989). Phosphatic clasts with flattened disc shape vary in size from <10 mm to >10 cm and are composed of phosphate and carbonate cemented quarzitic silt to fine sand. The P_2O_5 concentrations of the Kallavere Formation vary from 6 to 20 wt.% (Raudsep, 1997), in some coquina lenses, the P_2O_5 concentration can be as high as 30 wt.% (Baturin and Ilyin, 2013). The phosphatic sandstone is typically weakly cemented and friable, although in some localities it is cemented by dolomite (Raudsep, 1987).

The shelly phosphorites were likely deposited under conditions similar to modern Namibian shelf where abundant phosphatic lingulate (mainly *Discinisca tenuis*; Hiller, 1993) shell-rich sediments are found along the coast and organic rich sediments with authigenic sedimentary phosphate on the inner-shelf. By analogy with the Namibian shelf, the coquinas and bioclastic lenses in cross-bedded sandstones of the Kallavere Formation were formed in a high-energy shoreline-peritidal environment, whereas the intercalating and overlying graptolitic carbonaceous mudstones were formed under oxygen-poor deep(-er) water conditions (Hiller, 1993). High abundance of apatite secreting fossils and authigenic apatite cemented clasts as well as the presence of organic rich sediments point towards nutrient-rich conditions and high primary productivity (Baturin and Ilyin, 2013), consistent with the development of an upwelling ecosystem during the deposition of Kallavere phosphorites (Hiller, 1993; Lécuyer et al., 1998; Parrish et al., 1986). By the onset of the Paleozoic, the Baltica paleocontinent was positioned at 40-50° southerly latitudes and drifted (< 10 cm/yr) towards the tropics between the Early Ordovician and Mid-Silurian, reaching near equatorial latitudes by the Late Silurian (Torsvik et al., 2012). During the deposition of the Kallavere Formation in Furongian-Tremadocian, the Baltica paleocontinent was situated at high to intermediate southern latitudes (Torsvik et al., 2012) with the meridionally oriented shoreline of the Baltic Paleobasin facing towards the west, analogous to modern day Namibian shelf.

Peritidal Kallavere phosphorite deposits were rapidly transgressed by the overlying up to 7 m thick carbonaceous mudstones (so-called *Dictyonema* or graptolite shale) of the Türisalu Formation (Artyushkov et al., 2000; Heinsalu and Viira, 1997) enabling the preservation of these otherwise erosion-prone deposits (Sturesson et al., 2005). In some localities at the

southern margin of the phosphorite deposit, the shales of the Türisalu Formation are absent, and the Kallavere Formation is unconformably overlain by glauconitic sand- and siltstones of the Tremadocian-Floian Leetse Formation. In these areas, the phosphatic shells have a distinct red color due to the presence of hematite instead of secondary pyrite commonly present within the shells in areas where the phosphorite is overlain by carbonaceous mudstones.

Post-depositional history of Estonian phosphorites is marked by relative stability and subsequent low deposition rates. Despite their age, the phosphorites are largely unconsolidated and friable, indicating shallow burial and immature thermal maturation state. Low conodont alteration indices (CAI = 1-1.5; Heinsalu et al., 2003) of the Kallavere Formation further prove the relatively pristine state of the sediments. Therefore, it is likely that these rocks have not experienced any significant hydrothermal/late-diagenetic overprinting.

3. Material and Methods

Samples of the Kallavere Formation phosphorite were collected from four outcrops (Iru, Ülgase, Maardu, Saka localities) along the north Estonian coastline and from several drill cores penetrating the phosphorite beds in Toolse and Kabala deposits (Fig. 1).

For bulk analysis of trace element concentrations (including REE+Y) the phosphatic shell fragments were handpicked from phosphorite samples, cleaned with milliQ water and 2%$_{w/w}$ ultrapure HNO_3 solution in an ultrasonic bath (1 h for both reagents) to remove terrigenous and other non-apatitic components. After cleaning, samples were dissolved in concentrated HNO_3 for ICP-MS analysis. Trace elemental concentrations were measured using Agilent 8800 quadrupole ICP-MS. Indium was used as internal standard and NIST 1640a, NIST 1643f and POLC-1 as quality control standards.

For *in situ* trace-element measurements the bulk rock pieces and hand-picked single phosphatic brachiopod shells and clasts were embedded in Spurr`s epoxy resin and polished. In some samples it was possible to determine paleontological affinity of the shells to either *Ungula ingrica*, *Ungula inornata*, *Schmidtites celatus* or *Keyserlingia buchii* species's. The *Ungula ingrica* was the dominant species in all samples and the shells of this species were selected for comparative *in-situ* REE+Y analysis using specimens from different localities. In

addition, in Maardu locality both *Ungula ingrica* and *Ungula inornata* specimens were sampled to test the REE+Y concentration variability between species from the same locality.

Zeiss EVO MA15 variable pressure scanning electron microscope (SEM) coupled with an Oxford X-MAX energy dispersive detector system (EDS) was used to study the structure and major elemental composition of the samples. Trace element concentrations in individual shells and their different structural layers were measured with laser ablation inductively coupled plasma mass spectrometry (LA-ICP-MS) using an Agilent 8800 quadrupole ICP-MS coupled to a Cetac LSX- 213 G2+ laser with HelEx II fast-washout two-volume large-format cell. LA-ICP-MS raw data were transformed to elemental concentrations, using ^{43}Ca as an internal standard, assuming a stoichiometric concentration of Ca in apatite (39.7 wt.%). Additional standardization was performed using an external standard GSD-1G, with values from Jochum et al. (2011).

For spot analysis, a spot size of 25 µm, 10 Hz frequency and fluence of 2 J/cm^2 was used. Trace elemental mapping was done using the following parameters: 20 µm, 10 µm/s, 10 Hz and 1.3 J/cm^2, for spot size, scan speed, frequency and fluence, respectively. During LA-ICP-MS analysis, Ba-oxide interferes with Eu signal, and LREE oxides interfere with the HREE (Kent and Ungerer, 2005). The rate of Ba- and LREE-oxide formation was monitored with Th-oxide formation during ablation, which was <0.25% ThO/Th throughout the analytical sessions.

Post Archean Australian Shale values (PAAS; Taylor and McLennan, 1985) were used to normalize measured REE+Y concentrations. REE+Y based proxies were calculated as: $Eu/Eu^* = Eu_N/((Sm_N + Gd_N)/2)$, $Ce/Ce^* = Ce_N/(0.5La_N + 0.5Pr_N)$, $Pr/Pr^* = Pr_N/(0.5Ce_N + 0.5Nd_N)$, $Y/Y^* = Y_N ((Dy_N + Ho_N)/2)$, and $Gd/Gd^* = Gd_N/(Eu_N + Tb_N)/2)$ (Bau and Dulski, 1996; Byrne and Sholkovitz, 1996). To assess the degree of middle REE (MREE - Sm, Eu, Gd, Tb and Dy) enrichment, bell shape index (BSI) was calculated as: $BSI = (2*(Sm_N + Gd_N + Dy_N)/3)/ ((La_N + Pr_N + Nd_N)/3 + (Ho_N + Er_N + Tm_N + Yb_N + Lu_N)/5)$ (Tostevin et al., 2016). Subscript N denotes PAAS-normalized values for a given element.

To test the variability in the measured REE+Y concentrations between different localities, ANOVA and Tukey (HSD) tests were applied. RStudios was used for the analysis, and the significance level was set at $\alpha = 0.05$.

4. Results

4.1. Microscopy

The apatite in Estonian shelly phosphorites occurs in three forms: (i) abundant biogenic brachiopod shells and their fragments, (ii) early diagenetic cement occurring in reworked clasts and (iii) coatings on quartz grains and the occasional pore-fillings (Fig. 2).

The brachiopod shells vary in size from ~100 μm fragments rounded to a different extent, to >1 cm-size nearly intact valves (Figs. 2a-b). Some shells show signs of plastic deformation (Fig. 2f). The internal structure of the shells consists of alternating layers of baculate and compact laminae that are composed of trellised apatitic rods (bacula) and tightly packed apatite crystallites, respectively (Lang and Puura, 2013; Lang et al., 2016; Fig. 2e). The baculate laminae are often inter-grown with diagenetic pyrite aggregates (Fig. 2g) that give the shells a dark brown to black colour. Shells from Kabala area are pale to reddish in colour due to secondary hematite films and diffuse aggregates intruding the fractured shells (Fig. 2h). The phosphatic clasts are made up of angular to sub-angular silt to fine-sand quartz grains, embedded in apatite cement. The size range for flattened clasts is similar to the shells, typically ranging from sub-mm to >1 cm. Some clasts contain shell fragments (Fig. 2d) and in some of the clasts the quartz grains are coated in pyrite. Apatite grain coatings on quartz and the pore-filling apatite cements (Fig. 2c) are less dominant but were found in all localities sampled.

4.2. Trace elements

The average REE concentrations in shells is 1115.7 (SD = 591.4, n = 31) mg/kg, with a maximum and minimum value of 2415.3 mg/kg and 162.7 mg/kg, respectively (Table 1). The *in-situ* LA-ICP-MS analyses and elemental maps show heterogeneous distributions of REE+Y in individual shells (Figs. 3-4). The compact laminae of shells can contain up to tenfold higher REE+Y concentrations than baculate laminae (Figs. 5, 6a). However, the baculate laminae close to the outer surfaces and/or margins of the shell tend to show higher REE+Y concentrations than the internal baculate laminae (Figs. 3,5). In contrast to REE+Y, uranium shows systematically higher concentration in baculate laminae (Fig. 6b), dissimilarly to the REE+Y (Fig. 3). However, the principal shape of the PAAS normalized REE+Y patterns does not vary between the different shell fragments of the same or different species

form the same locality, or between the structural layers nor along the same structural layer within a single shell (Figs. 5,7; Table 1).

Principally, two types of patterns can be recognized in the studied samples – patterns with moderate to high degree of MREE-enrichment (e.g., Saka, Iru) and seawater and/or shale like patterns (Maardu, Kabala; Fig. 7). The REE concentrations are the lowest and the most PAAS-like in shells from Kabala locality but show typically wedge shape patterns in shells from other localities, with REE+Y concentrations showing around tenfold enrichment relative to PAAS (Fig. 7). Tukey's HSD Test for multiple comparisons shows that the mean value of REE+Y concentrations are significantly lower in Kabala compared to all other localities except Maardu, at $p < 0.001$ level. Similarly, REE+Y concentrations in Saka locality are significantly higher compared to other localities, whereas there are no statistically significant differences in REE+Y concentrations between Iru, Ülgase and Toolse localities. MREE-enrichment is apparent in samples from all localities (less so in Maardu and Kabala), with an average BSI of 1.55 (SD = 0.20, n = 31). BSI and ∑REE show moderate correlations ($r = 0.61$, p-value <0.01, n = 31), with the highest BSI values corresponding to the highest REE concentrations (Fig. 8). Ce/Ce* values range from 0.72 to 1.04 (Fig. 9), with an average value of 0.95 (SD = 0.08, n = 31). Eu/Eu* values are stable in all samples, with values ranging from 0.79-1.05. In contrast, Y/Ho ratios show significant variability, with values ranging from >50 to ~30 (Fig 10). Average La_N/Yb_N, La_N/Sm_N and La_N/Nd_N ratios are 1.02 (SD = 0.14, n = 31), 0.77 (SD = 0.24, n = 31), 0.85 (SD = 0.26, n = 31), respectively (Table 1).

Phosphatic clasts are typically more REE+Y enriched compared to shells from the same locality (Fig. 11; Table 1). In Maardu locality, the average ∑REE in shells is 569.5 mg/kg (SD = 201.85, n = 4), whereas the ∑REE in a phosphatic clast is 1000.6 mg/kg. On the other hand, REE concentrations are lower in clasts than the shells in the Iru formation (Fig. 11). In phosphatic clasts the most REE+Y rich zones are associated with thin apatite films that were precipitated directly onto the quartz grains, whereas the bulk of the apatite cement has comparatively lower REE+Y (Fig. 4).

5. Discussion

5.1. Locality-based variability of REE+Y in phosphorites

The REE content in extant linguliform brachiopods is very low with ∑REE typically around 1 mg/kg and rarely up to 10 mg/kg (Lécuyer et al., 1998; Shaw and Wasserburg, 1985). The maximum ∑REE concentration in Estonian shelly phosphorites measured in this study reached values up to 2415 mg/kg, and REE concentrations as high as ~2 wt.% have been reported in some sedimentary apatites (Emsbo et al., 2015). It is well established that such vast enrichment with factors of more than 10^7 compared to seawater is driven by diagenetic processes (Shields and Webb, 2004). The REE and Y replace Ca ions in the apatite structure by pairwise substitution mechanism where one REE^{3+} together with one monovalent ion (e.g., Na^+) replace two Ca^{2+} ions (Jarvis et al., 1994; Pan and Fleet, 2002). Alternatively, the Ca^{2+} and P^{5+} can be substituted by REE^{3+} and Si^{4+} (Pan and Fleet, 2002).

Seawater is considered as a common source of REEs for bioapatites (e.g., Girard and Lécuyer, 2002; Herwartz et al., 2013; Reynard et al., 1999) and the REE concentrations of nascent apatite reflect, similar to biogenic carbonates and pure carbonate muds, seawater signals (Barrat et al., 2000; Elderfield and Pagett, 1986; Lécuyer et al., 2004; Webb et al., 2009). The PAAS normalized REE+Y distribution pattern of modern oxygenated seawater is characterized by progressive enrichment from LREE to HREE, negative Ce anomalies (de Baar et al., 1985), slight positive La and Gd anomalies (Bau, 1999), and a Y/Ho ratio of >52 (Nozaki et al., 1997). However, numerous studies have inferred that the composition of the bioapatite is significantly modified at shallow burial and most of the REE+Y is taken up during early diagenetic open-system processes where elevated pore-water REE+Y concentrations are sourced from clays, organic matter mineralization and Fe-Mn oxyhydroxide reduction (Abbott et al., 2019; Chen et al., 2015; Deng et al., 2017; Herwartz et al., 2013; Zhao et al., 2013). As a result of differences in the rates of diagenetic processes, the PAAS normalized REE+Y patterns of sedimentary apatites can be divided into three broad groups: (i) seawater-like patterns, mainly characterized by negative Ce-anomalies, varying degree of HREE-enrichment and super-chondritic Y/Ho ratios (Emsbo et al., 2015; Shields and Stille, 2001) (ii) shale-like patterns with small or absent Ce-anomalies, little to no HREE enrichment and (near-)chondritic Y/Ho ratios (Emsbo et al., 2015; Lumiste et al., 2019; McArthur and Walsh, 1984) and (iii) "bell shaped" MREE-enriched patterns, with no Ce anomalies, and depletion of both LREE and HREE (Reynard et al., 1999; Shields and Stille, 2001). Typically, the REE+Y concentrations of these three types increase from seawater-like to bell shape patterns, with flat PAAS normalised pattern representing an intermediate state between the two endmembers (e.g., Lécuyer et al., 2004; Lumiste et al., 2019). While

enrichments in apatite not exceeding the 10^7 threshold compared to seawater concentrations exhibit seawater-type REE+Y characteristics consistent with quantitative uptake (i.e., the shape of the typical seawater pattern is preserved), higher REE enrichments associating with distinct bell shape patterns reflect either crystal-chemical controls that cause preferential partitioning of MREE during extensive diagenetic alteration (Reynard et al., 1999) or uptake from MREE-enriched anoxic pore-water (Kocsis et al., 2009; Ounis et al., 2008).

The PAAS normalized REE+Y patterns of the Estonian shelly phosphorites in all localities, except in Kabala and Maardu, are characterized by MREE enrichment, with bell shape index (BSI) values up to 1.55. BSI also correlates with ∑REE ($r = 0.61$, p-value <0.01, $n = 31$; Fig. 8a), pointing towards an anoxic pore-water source for the REE+Y. Similarly, the decrease in La_N/Nd_N (Fig. 12) and Y/Ho (Fig. 10) ratios with increasing ∑REE further supports the non-marine pore-water source for the REE. The Y/Ho ratios of Maardu samples show values close or even somewhat higher than the average modern seawater, whereas samples from nearby Iru and Ülgase localities (located within ca. 5 km radius from Maardu outcrop) show values close to chondritic Y/Ho ratio (Fig. 10). Y and Ho have a very similar ionic radii but Ho is preferentially scavenged from seawater column by particulate matter or ionic species resulting in high (>50) seawater Y/Ho ratios, distinctly higher than the typical Y/Ho ratios of 25–30 in shales (Bau and Dulski, 1996; McLennan, 2001). Decreasing Y/Ho ratios with increasing ∑REE in Estonian shelly phosphorite suggest dominant lithogenic source of REEs in phosphatic shells. If the variation of the Y/Ho ratios in Estonian shelly phosphorite were due to contributions from two end-members – seawater and a lithogenic components with Y/Ho ratios of 60 and 28, respectively – then the share of lithogenic fraction in most samples is >50%.

Significant diagenetic overprinting is also evident in Ce/Ce* values that typically are in the 0.7 – 1 range, although a true negative Ce-anomaly (*sensu* Bau and Dulski, 1996) was found in only one ICP-MS sample (Fig. 9). REE composition of extant lingulates is characterized by strong negative Ce anomaly expressing the composition of oxygenated seawater (e.g., Lécuyer et al., 1998). This anomaly is progressively diminished and, in some cases, replaced by a positive Ce anomaly during REE uptake from diagenetically modified pore-water enriched in Ce. Indeed, some Estonian phosphorite samples do show true positive Ce anomaly, possibly indicative of Ce uptake from suboxic pore-water enriched in REE+Y due to the reductive dissolution of Fe-Mn particles (Takahashi et al., 2015).

The La_N/Yb_N and La_N/Sm_N values fall outside the range of modern seawater, indicating a diagenetic source for the majority of REE+Y (Fig. 13). Diagenetic uptake via adsorption mainly increases the La_N/Yb_N ratios, whereas the substitution mechanism should lead to decrease in La_N/Sm_N ratios (Reynard et al., 1999). All measured samples show higher than seawater La_N/Yb_N ratios indicating that the prevalent uptake mechanism was adsorption. Substitution mechanism could be still suggested for some samples, particularly the ones with the highest REE+Y content (Fig. 13). Both extensive recrystallization during late-stage diagenesis (Reynard et al., 1999) and uptake from anoxic pore-water (Kocsis et al., 2009; Ounis et al., 2008) can lead to the development of MREE-enrichment (i.e. high BSI, low La_N/Sm_N), making it difficult to unambiguously trace the source and the uptake mechanism of the REE+Y in apatite. However, extensive late diagenetic uptake is typically accompanied by low La_N/Sm_N ratios (<0.3; Lécuyer et al., 2004; Reynard et al., 1999), lower than the values measured from our samples (0.47-1.53; Fig, 13), pointing towards early diagenetic uptake from anoxic pore-water (Haley et al., 2004). Furthermore, Y/Y* and La_N/Nd_N ratios (Fig. 12) show a positive co-variation with a trend towards diagenetic enrichment, except in a few shells from Kabala and Maardu localities that potentially show weathering influences, which preferentially remove non-tetrad REE (Shield and Stille, 2001).

The studied phosphorite bearing sequences consist of similar medium-to-coarse grained shallow marine quartzose sandstone with abundant phosphatic shell fragments and, while samples from the same localities display remarkably uniform REE content and REE+Y patterns, the variability between different localities can be rather large. The ten-fold difference in REE concentrations of shells from different localities, that are only few tens of km apart, could have been caused both by syn-depositional and early diagenetic (e.g., input of REE+Y carrying phases, sedimentary environment) and/or post-depositional (e.g., metamorphism, weathering, hydrothermal alteration) processes (Bau, 1991; Bonnand et al., 2020). Redistribution of REE+Y during late-stage diagenesis and metamorphism is largely controlled by the stability of the host-phases but large-scale redistribution of bulk rock REE+Y is rare (Chakrabarti et al., 2007; Ohr et al., 1994), unless influenced by hydrothermal alteration (e.g., Chetty and Gutzmer, 2012). Resetting of the REE+Y signatures due to hydrothermal alteration in Estonian shelly phosphorite seems unlikely given the overall tectonic stability and shallow burial of the sedimentary sequences in the northern Baltica Paleobasin with only limited evidence for hydrothermal activity (Eensaar et al., 2017; Gaškov

et al., 2017; Somelar et al., 2010), excellent preservation of conodonts with CAI values <1.5 (Heinsalu et al., 2003), and the absence of Eu-anomalies, that would be indicative of Eu^{2+}/REE^{3+} decoupling in high temperature (>200 °C) processes (Bau et al., 2010).

However, even in sediments not influenced by hydrothermal activity, protracted uptake of REE+Y by biogenic apatite can still occur during late-stage diagenesis (Herwartz et al., 2011; Kowal-Linka et al., 2014) and can, in some cases, account for >50% of the REE found in apatite (Kocsis et al., 2010). Therefore, the apparent locality-based differences in REE+Y concentrations in the studied samples could have, theoretically, been caused by differences in the availability of these elements during late-stage diagenesis. Well-crystallized biogenic apatite is less susceptible to late-stage diagenesis (Kocsis et al., 2010) and recrystallization rates influence REE+Y fractionation in biogenic apatite (Trueman et al., 2011). Considering that the early diagenetic apatite in compact layers of the shells (Lang et al., 2016) contain more REE+Y (Fig. 5) than the porous authigenic baculate layers, it is unlikely that the majority of these elements could have been incorporated during late-stage diagenesis. Moreover, if a large portion of the REE+Y were taken up during late-stage diagenesis – i.e. the REE+Y composition of the shells would be a mixture of both early and late-stage diagenetic pore-water – the shells would display internal variability (Herwartz et al., 2013). Measurements from a single shell (Fig. 5), however, display remarkable uniformity between compact and baculate laminae REE+Y patterns. Although the precise timing of REE+Y uptake is difficult to constrain and late-stage diagenetic contribution cannot be fully ruled out, it is unlikely that late diagenetic fluids served as the predominant source of REE+Y in the shells.

The only significant difference of the shells with varying REE+Y content is their colouring – dark brown-to-black shells are higher in ∑REE and light brown pale-to-reddish shells are lower in ∑REEs. The colouring of the shells is due to the presence of secondary pyrite or hematite in black and pale-reddish shells, respectively. Diagenetic pyrite impregnating the shell structures (Fig. 2) is a common secondary phase in phosphorites northern and western areas, whereas in Kabala area the pyrite is largely absent and hematite is the dominant Fe-containing phase (Nemliher and Puura, 2001). The Fe speciation in shells likely reflects the redox state of pore-water during early diagenesis – pyrite inter-grown brachiopods experienced the development of sulfidic early diagenetic pore waters, whereas the presence of hematite is indicative of oxic to suboxic pore-water conditions. Alternatively, the hematite

could be the result of oxidation of diagenetic pyrite by percolating meteoric water. As such, the putative remobilization of REE+Y by meteoric water could explain the much lower ∑REE values in the "hematitic" shells from Kabala phosphorites. Deep ground-waters, even if influenced by REE-rich lithologies, are characterized by REE+Y concentrations in the range of ng/L (Munemoto et al., 2015). These low concentrations would likely allow at least some of the REE+Y to be leached out of the apatite, resulting in REE+Y depletion from the surfaces of the shells and phosphatic clasts. However, the elemental distributions in shells from Kabala locality show that the highest REE+Y concentrations are found in the outer margin of the shells (Fig. 3), which is more in line with diagenetic REE+Y uptake (e.g., Lumiste et al., 2019) rather than leaching and removal of these elements. Therefore, it can be suggested that lower ∑REE values in Kabala do not result from secondary mobilization and removal of these elements but rather reflect limited REE+Y uptake/availability during digenesis at or near the SWI.

It is interesting that the REE+Y content is particularly low in shells in the southernmost part of the phosphorite deposit where overlying carbonaceous mudstone ("graptolite mudstone") of the Türisalu Formation is missing in the stratigraphy and the Kallavere Formation is directly overlain by glauconitic sand- and siltstones of the Leetse Formation. It is possible that post depositional remobilisation of REE+Y from overlying carbonaceous mudstone, that has been documented in other basins (e.g., Lev and Filer, 2004), could be considered as a potential REE+Y source for phosphatic shells and would explain the substantial heterogeneity of REE+Y concentrations of different localities. The shell bearing quartz sandstones of the Kallavere Formation themselves were deposited in hydrodynamically active setting and do not contain significant clay/mud material and, therefore, present a poor (internal) source for REE+Y. However, the REE+Y in the lenses of black shales intercalating the sandstones of the Kallavere Formation and particularly in the carbonaceous mudstones of the overlying Türisalu Formation could have been mobilized during early diagenesis and taken up by phosphatic shells.

Alternatively, the highly location specific variability of REE+Y concentrations in Estonian shelly phosphorite could have been controlled by the availability of these elements in ambient seawater and/or pore fluids shortly after deposition. Concentrations of REE+Y in modern marine settings vary significantly, for example, a 2.5-fold differences in dissolved REE concentrations are found between the Northern Pacific and Atlantic oceans (de Baar et al.,

2018). Similarly, REE+Y concentrations vary within a single basin, with significant variability between near-shore margins, slope and basin (Deng et al., 2017). Dissolved REE+Y concentrations (excluding Ce) in seawater tend to increase with water depth (Deng et al., 2017; De Baar et al., 2018). In pore-water, however, the REE concentrations increase even more, peaking at the SWI or a few centimetres below (Abbott et al., 2015; Deng et al., 2017; Haley et al., 2004). This is caused by reductive dissolution of organic matter and Fe-Mn oxyhydroxides (Abbott et al., 2015; Haley et al., 2004) and/or dissolution and authigenesis of clay minerals (Abbott et al., 2019) releasing REE+Y to the pore-water during early diagenesis and result in concentrations at least an order of a magnitude higher than the overlying water column (Abbott et al., 2015). The freshly liberated REE+Y diffuse back to the overlying water column (Deng et al., 2017) or are taken up by suitable secondary minerals (Abbott et al., 2019). Given that the majority of these processes occur during early diagenesis, REE+Y concentrations drop rapidly with increasing sediment depth, resulting in deep pore-water being depleted in REE+Y (Soyol-Erdene and Huh, 2013). Furthermore, redox conditions exhibit control on pore-water REE+Y concentrations and can cause both increase (i.e., by Fe-Mn oxyhydroxide and organic matter dissolution) and decrease (e.g., by authigenic apatite formation) in pore-water REE+Y concentrations. The most intensive release of particle bound REE+Y and high REE+Y fluxes are related to anoxia (Deng et al., 2017). The Namibian shelf – a modern day analogue to the Baltic basin during the early Palaeozoic (Hiller, 1993) – is characterized by highly dynamic redox conditions related to upwelling and respiration (Brüchert et al., 2006). High flux of organic matter and its subsequent degradation can lead to the development of local transient anoxia, deposition of organic rich muds and phosphogenesis (Baturin, 2000; Lumiste et al., 2021), while predominantly oxic conditions can prevail in other areas on the shelf (Brüchert et al., 2003). This type of dynamic redox conditions or “poikiloxia” (Algeo and Rowe, 2012) may result in spatially variable REE+Y concentrations in pore-waters even in sediments across short distances, with low pore-water concentrations in sediments with dominantly oxic conditions and REE+Y enriched pore-waters under anoxic conditions (Fig. 14). Poikiloxia could lead to highly variable and mosaic REE+Y distribution in otherwise coeval sediments and could, thus, explain the lateral variability of the REE+Y enrichments in Estonian shelly phosphorite.

5.2. Heterogenous distribution of REE+Y in phosphatic shells and clasts

Distribution of the REE+Y in Estonian phosphatic fossil lingulate shells is also highly heterogeneous at the individual shell level (Figs. 3,5). The highest REE+Y concentrations are

found in the periphery/outer surfaces of the shells, whereas the content of REE+Y is up-to an order of magnitude (typically about 3-5 times) lower in centre of the shells (Fig. 3). Furthermore, the compact laminae commonly display a higher concentration of REE+Y than the baculate laminae (Figs. 3,5). Alternating fossilised compact and baculate laminae (Fig. 2) represent the inner structure of the extant lingulate brachiopod shells that were deposited as highly mineralized laminae alternating with laminae rich in organic matrix (Williams and Cusack, 2007, 1999). The compact laminae are composed of closely packed apatite nanocrystals secreted by the animal and the baculate laminae are composed of trellised apatitic rods (bacula), which during the lifetime of the brachiopod were enmeshed into an organic matrix (Lang et al., 2016; Lang and Puura, 2013; Williams and Cusack, 1999).

Biogenic apatite of the lingulate shells is readily recrystallized *post-mortem* due to relatively high degree of structural disorder and small crystallite sizes (Lang et al., 2016; Lang and Puura, 2013; Nemliher and Puura, 2001)**.** However, the apatite in compact laminae was interpreted by Lang et al. (2016) as an early diagenetically recrystallized skeletal apatite, which has preserved some of its original characteristics like low F-content, nanometer-scale crystallite size and apatite crystal structure lattice parameter values similar to the apatite in modern lingulate brachiopod shells. Extant brachiopods, unlike other animals with hydroxyapatite skeleton, precipitate carbonate and fluoride enriched form of apatite that is similar to carbonate-fluorapatite (Neary et al., 2011), which is thermodynamically more stable under marine and pore-water conditions (Jahnke, 1984) and could be preserved through geological time with only minor modifications. The baculate laminae in lingulates from Estonian shelly phosphorites, in contrast, represent non-skeletal, mostly authigenic apatite (Nemliher and Puura, 2001) that show higher CO_3^{2-} and F^- content and are characterized by well crystalline micrometer–size crystallite frameworks (Lang et al., 2016). The phosphatization of the organic rich mesh likely happened relatively early, possibly concomitantly with the degradation of organic matter by microbial sulfate reduction (Lécuyer et al., 1998) as evidenced by partially preserved fragile organic frameworks (Lang and Puura, 2013) and close association with diagenetic pyrite (Lang et al., 2016).

The phosphatic shells of the Estonian phosphorite are, in composition, similar to modern authigenic sedimentary apatites (*sensu* Mänd et al., 2018) that form at the SWI (Lumiste et al., 2021) on the Namibian Shelf. REE+Y enrichment in these modern phosphatic sediments occurs through the dominant adsorption mechanism in diagenetically modified pore-water

utilizing REE+Y released by organic matter degradation, reduction of Fe-Mn oxyhydroxides and detrital clay phases gradually diminishing the seawater characteristics with increasing ∑REE (e.g., Lumiste et al., 2019). The comparatively higher REE+Y concentration in compact laminae of Estonian phosphatic shells could be thus explained by higher surface area and therefore more effective REE+Y uptake by the nanometer-size apatite crystallite aggregates. In contrast to the REE+Y, U content is remarkably higher in baculate laminae (see Fig. 3, 6). U is mostly taken up into apatite structure as U^{4+} via substitution with Ca^{2+} (Pan and Fleet, 2002). As U^{4+} is the dominant species in reduced depositional environments (Barnes and Cochran, 1990), and the phosphatization of the baculate laminae is possibly tied to the mineralization of the organic matter and establishment of (at least) locally reduced environments required for stabilization of pyrite, it is likely that U in Estonian shelly phosphorite was fixed in baculate laminae of shell structure during early diagenesis. The heterogeneity between the external and internal parts of the shell can be most plausibly explained by enhanced ion-exchange and diffusion between REE+Y-rich fluids (either seawater or pore-water) and the exterior of the shells, similar to modern day REE+Y uptake in phosphogenic sediments (Lumiste et al., 2019).

The less prevalent apatite bearing constituents in Estonian shelly phosphorite are allochthonous flat/rounded phosphatic clasts, and *in-situ* grain coatings. The clasts are made of carbonate and apatite cemented poorly rounded fine-sand to coarse-silt grain size quartz aggregates that were likely transported to a shallow shore-face environment during singular high energy event (i.e., storms) when the wave base was low enough to move sediments from the middle-or-inner shelf to near-shore facies. The REE+Y patterns of phosphatic clasts exhibit MREE-enrichment, absence of Eu- or Ce-anomalies and lower than seawater Y/Ho ratios (average 44.5, SD = 3.9, n = 3), and rather low ∑REE (average 824.8 mg/kg, SD = 247.6, n = 3). Similar to the shell fragments, the REE+Y distribution in the phosphatic clasts and grain coatings is heterogenous and the highest REE+Y content is found at the outer margin of the clasts and in phosphatic grain coatings precipitated immediately onto quartz grains, whereas the centres of the clasts have significantly lower REE content. Similar clasts of apatite cemented fine sandstone with similar REE+Y content and MREE enrichment are described across the lower–middle Cambrian transition in Scania, southern Sweden (Álvaro et al., 2016) that were possibly sourced from apatite-cemented sandstones and hardgrounds described, for example, in the Vassbo area in central Sweden (Wallin, 1989). The source area of the apatite cemented clasts in the Estonian shelly phosphorite is not known but the

development of such phosphatized sediments could be similar to the sedimentary phosphorite deposition on the modern Namibia and Peru inner shelf where high rates of primary production and subsequent degradation of the resulting organic matter leads to fluctuating redox conditions near the seafloor apatite precipitation at SWI (Arning et al., 2009a; Brock and Schulz-Vogt, 2011; Brüchert et al., 2000; Compton and Bergh, 2016; Goldhammer et al., 2010; Lumiste et al., 2021), The REE+Y occurrence in phosphatic clasts (Fig. 4) mirrors their distribution in biogenic shells, suggesting that the REE+Y enrichment was likely coeval in both apatite phases and happened during early diagenetic stage through the scavenging of REE+Y released into pore-water.

Conclusions

REE concentrations in Paleozoic shelly phosphorites of Estonia vary from 162.7 to 2415.3 mg/kg, with significant variability between localities only a few tens of km apart. For example, Saka locality phosphorites contain up to 14 times more REE than the Kabala locality. PAAS normalised REE+Y patterns also vary between localities, with shale-like patterns in the REE+Y depleted localities and bell-shaped patterns in REE+Y enriched localities. ∑REE and BSI show moderate correlation ($r = 0.61$, p-value <0.01, $n = 31$), pointing towards a diagenetic source for these elements. Y/Ho ratios range from >50 to around 30, signalling a gradual loss of seawater signatures during diagenetic REE+Y enrichment. La_N/Yb_N and La_N/Sm_N ratios of the phosphorites resemble marine pore-water values, further implicating the role of early diagenetic uptake of the REE+Y.

In addition to locality-based variability, the distribution of REE+Y within the shells of phosphatic brachiopods is heterogeneous. Typically, the diagenetically altered compact laminae of skeletal origin contain more REE+Y, whereas the baculate laminae – composing mostly of phosphatized authigenic remnants of organic rich meshes – contain less REE+Y. Dissimilarly, the baculate laminae contain more U than compact laminae. Although there is variability between the different types of apatite found in the shells, the most substantial variation is related to the spatial distribution of REE+Y in the shells, with the highest concentrations found in the periphery of shells. Besides phosphatic shells, the phosphorites contain phosphatic clasts and *in-situ* grain coatings. The REE+Y distribution in the clasts resemble biogenic shells, pointing towards a uniform source for these elements. The internal distribution trends of REE+Y in the shells and clasts, high BSI, pore-water-like La_N/Yb_N,

569 La_N/Sm_N ratios and the mosaic variability of REE+Y concentrations in different localities are
570 most parsimoniously explained by dynamic redox conditions controlling the availability of
571 REE+Y in pore-water during early diagenetic transformation of the shells and clasts.

572 **Acknowledgements**

573 The authors would like to thank Tõnn Paiste, Karin Kungla, Lauri Joosu and Johannes Vind
574 for their help with sampling. This study was supported by Estonian Science Agency project
575 RESTA19 and Estonian Centre of Analytical Chemistry.

576 **References**

577 Abbott, A.N., Haley, B.A., McManus, J., Reimers, C.E., 2015. The sedimentary flux of
578 dissolved rare earth elements to the ocean. Geochim. Cosmochim. Acta 154, 186–200.
579 https://doi.org/10.1016/j.gca.2015.01.010
580 Abbott, A.N., Löhr, S., Trethewy, M., 2019. Are Clay Minerals the Primary Control on the
581 Oceanic Rare Earth Element Budget? Front. Mar. Sci. 6, 1–19.
582 https://doi.org/10.3389/fmars.2019.00504
583 Algeo, T.J., Rowe, H., 2012. Paleoceanographic applications of trace-metal concentration
584 data. Chem. Geol. 324–325, 6–18. https://doi.org/10.1016/j.chemgeo.2011.09.002
585 Álvaro, J.J., Shields-Zhou, G.A., Ahlberg, P., Jensen, S., Palacios, T., 2016. Ediacaran–
586 Cambrian phosphorites from the western margins of Gondwana and Baltica.
587 Sedimentology 63, 350–377. https://doi.org/10.1111/sed.12217
588 Arning, E.T., Birgel, D., Brunner, B., Peckmann, J., 2009a. Bacterial formation of phosphatic
589 laminites off Peru. Geobiology 7, 295–307. https://doi.org/10.1111/j.1472-
590 4669.2009.00197.x
591 Arning, E.T., Lückge, A., Breuer, C., Gussone, N., Birgel, D., Peckmann, J., 2009b. Genesis
592 of phosphorite crusts off Peru. Mar. Geol. 262, 68–81.
593 https://doi.org/10.1016/j.margeo.2009.03.006
594 Artyushkov, E.A., Lindström, M., Popov, L.E., 2000. Relative sea-level changes in
595 Baltoscandia in the Cambrian and early Ordovician: The predominance of tectonic
596 factors and the absence of large scale eustatic fluctuations. Tectonophysics 320, 375–
597 407. https://doi.org/10.1016/S0040-1951(00)00038-X
598 Auer, G., Reuter, M., Hauzenberger, C.A., Piller, W.E., 2017. The impact of transport
599 processes on rare earth element patterns in marine authigenic and biogenic phosphates.
600 Geochim. Cosmochim. Acta 203, 140–156. https://doi.org/10.1016/j.gca.2017.01.001

601 Barnes, C.E., Cochran, J.K., 1990. Uranium removal in oceanic sediments and the oceanic U
602 balance. Earth Planet. Sci. Lett. 97, 94–101. https://doi.org/10.1016/0012-
603 821X(90)90101-3
604 Barrat, J.A., Taylor, R.N., André, J.P., Nesbitt, R.W., Lecuyer, C., 2000. Strontium isotopes
605 in biogenic phosphates from a Neogene marine formation: Implications for
606 palaeoseawater studies. Chem. Geol. 168, 325–332. https://doi.org/10.1016/S0009-
607 2541(00)00200-X
608 Baturin, G.N., 2000. Formation and Evolution of Phosphorite Grains and Nodules on the
609 Namibian Shelf, from Recent to Pleistocene, in: Glenn, C.R., Prévôt-Lucas, L., Lucas, J.
610 (Eds.), Marine Authigenesis: From Global to Microbial. SEPM Society for Sedimentary
611 Geology.
612 Baturin, G.N., Ilyin, A. V., 2013. Comparative geochemistry of shell phosphorites and
613 dictyonema shales of the Baltic. Geochemistry Int. 51, 23–32.
614 https://doi.org/10.1134/S0016702913010023
615 Bau, M., 1999. Scavenging of dissolved yttrium and rare earths by precipitating iron
616 oxyhydroxide: Experimental evidence for Ce oxidation, Y-Ho fractionation, and
617 lanthanide tetrad effect. Geochim. Cosmochim. Acta 63, 67–77.
618 https://doi.org/10.1016/S0016-7037(99)00014-9
619 Bau, M., 1991. Rare-earth element mobility during hydrothermal and metamorphic fluid-rock
620 interaction and the significance of the oxidation state of europium. Chem. Geol. 93,
621 219–230. https://doi.org/10.1016/0009-2541(91)90115-8
622 Bau, M., Balan, S., Schmidt, K., Koschinsky, A., 2010. Rare earth elements in mussel shells
623 of the Mytilidae family as tracers for hidden and fossil high-temperature hydrothermal
624 systems. Earth Planet. Sci. Lett. 299, 310–316.
625 https://doi.org/10.1016/j.epsl.2010.09.011
626 Bau, M., Dulski, P., 1996. Distribution of yttrium and rare-earth elements in the Penge and
627 Kuruman iron-formations, Transvaal Supergroup, South Africa. Precambrian Res. 79,
628 37–55. https://doi.org/10.1016/0301-9268(95)00087-9
629 Birski, Ł., Słaby, E., Wirth, R., Koch-Müller, M., Simon, K., Wudarska, A., Götze, J.,
630 Lepland, A., Hofmann, A., Kuras, A., 2019. Archaean phosphates: a case study of
631 transformation processes in apatite from the Barberton greenstone belt. Contrib. to
632 Mineral. Petrol. 174, 1–23. https://doi.org/10.1007/s00410-019-1560-z
633 Bonnand, P., Lalonde, S. V., Boyet, M., Heubeck, C., Homann, M., Nonnotte, P., Foster, I.,
634 Konhauser, K.O., Köhler, I., 2020. Post-depositional REE mobility in a Paleoarchean

635 banded iron formation revealed by La-Ce geochronology: A cautionary tale for signals
636 of ancient oxygenation. Earth Planet. Sci. Lett. 547, 116452.
637 https://doi.org/10.1016/j.epsl.2020.116452
638 Brock, J., Schulz-Vogt, H.N., 2011. Sulfide induces phosphate release from polyphosphate in
639 cultures of a marine Beggiatoa strain. ISME J. 5, 497–506.
640 https://doi.org/10.1038/ismej.2010.135
641 Brüchert, V., Currie, B., Peard, K.R., Lass, U., Endler, R., Dübecke, A., Julies, E., Leipe, T.,
642 Zitzmann, S., 2006. Biogeochemical and physical control on shelf anoxia and water
643 column hydrogen sulphide in the Benguela coastal upwelling system off Namibia., in:
644 Neretin, L.N. (Ed.), Past and Present Water Column Anoxia. Kluwer Academic
645 Publishers, Dordrecht, pp. 161–193. https://doi.org/10.1007/1-4020-4297-3_07
646 Brüchert, V., Jørgensen, B.B., Neumann, K., Riechmann, D., Schlösser, M., Schulz, H., 2003.
647 Regulation of bacterial sulfate reduction and hydrogen sulfide fluxes in the central
648 Namibian coastal upwelling zone. Geochim. Cosmochim. Acta 67, 4505–4518.
649 https://doi.org/10.1016/S0016-7037(03)00275-8
650 Brüchert, V., Pérez, M.E., Lange, C.B., 2000. Coupled primary production, benthic
651 foraminiferal assemblage, and sulfur diagenesis in organic-rich sediments of the
652 Benguela upwelling system. Mar. Geol. 163, 27–40. https://doi.org/10.1016/S0025-
653 3227(99)00099-7
654 Byrne, R.H., Sholkovitz, E.R., 1996. Chapter 158 Marine chemistry and geochemistry of the
655 lanthanides. Handb. Phys. Chem. Rare Earths. https://doi.org/10.1016/S0168-
656 1273(96)23009-0
657 Chakrabarti, R., Abanda, P.A., Hannigan, R.E., Basu, A.R., 2007. Effects of diagenesis on
658 the Nd-isotopic composition of black shales from the 420 Ma Utica Shale Magnafacies.
659 Chem. Geol. 244, 221–231. https://doi.org/10.1016/j.chemgeo.2007.06.017
660 Chen, J., Algeo, T.J., Zhao, L., Chen, Z.Q., Cao, L., Zhang, L., Li, Y., 2015. Diagenetic
661 uptake of rare earth elements by bioapatite, with an example from Lower Triassic
662 conodonts of South China. Earth-Science Rev. 149, 181–202.
663 https://doi.org/10.1016/j.earscirev.2015.01.013
664 Chetty, D., Gutzmer, J., 2012. REE redistribution during hydrothermal alteration of ores of
665 the Kalahari Manganese Deposit. Ore Geol. Rev. 47, 126–135.
666 https://doi.org/10.1016/j.oregeorev.2011.06.001
667 Compton, J.S., Bergh, E.W., 2016. Phosphorite deposits on the Namibian shelf. Mar. Geol.
668 380, 290–314. https://doi.org/10.1016/j.margeo.2016.04.006

669 de Baar, H.J.W., Bacon, M.P., Brewer, P.G., Bruland, K.W., 1985. Rare earth elements in the
670 Pacific and Atlantic Oceans. Geochim. Cosmochim. Acta 49, 1943–1959.
671 https://doi.org/10.1016/0016-7037(85)90089-4
672 de Baar, H.J.W., Bruland, K.W., Schijf, J., van Heuven, S.M.A.C., Behrens, M.K., 2018.
673 Low cerium among the dissolved rare earth elements in the central North Pacific Ocean.
674 Geochim. Cosmochim. Acta 236, 5–40. https://doi.org/10.1016/j.gca.2018.03.003
675 de Baar, H.J.W., Schijf, J., Byrne, R.H., 1991. Solution chemistry of the rare earth elements
676 in seawater. Eur. J. Solid State Inorg. Chem. 28, 357–373.
677 Deng, Y., Ren, J., Guo, Q., Cao, J., Wang, H., Liu, C., 2017. Rare earth element
678 geochemistry characteristics of seawater and porewater from deep sea in western
679 Pacific. Sci. Rep. 7, 1–13. https://doi.org/10.1038/s41598-017-16379-1
680 Eensaar, J., Gaškov, M., Pani, T., Sepp, H., Somelar, P., Kirsimäe, K., 2017. Hydrothermal
681 fracture mineralization in the stable cratonic northern part of the Baltic Paleobasin:
682 sphalerite fluid inclusion evidence. Gff 139, 52–62.
683 https://doi.org/10.1080/11035897.2016.1196499
684 Elderfield, H., Pagett, R., 1986. Rare earth elements in ichthyoliths: Variations with redox
685 conditions and depositional environment. Sci. Total Environ. 49, 175–197.
686 https://doi.org/10.1016/0048-9697(86)90239-1
687 Emsbo, P., McLaughlin, P.I., Breit, G.N., du Bray, E.A., Koenig, A.E., 2015a. Rare earth
688 elements in sedimentary phosphate deposits: Solution to the global REE crisis?
689 Gondwana Res. 27, 776–785. https://doi.org/10.1016/j.gr.2014.10.008
690 Emsbo, P., McLaughlin, P.I., Breit, G.N., du Bray, E.A., Koenig, A.E., 2015b. Rare earth
691 elements in sedimentary phosphate deposits: Solution to the global REE crisis?
692 Gondwana Res. 27, 776–785. https://doi.org/10.1016/j.gr.2014.10.008
693 Felitsyn, S., Sturesson, U., Popov, L., Holmer, L., 1998. Nd isotope composition and rare
694 earth element distribution in early Paleozoic biogenic apatite from Baltoscandia: A
695 signature of Iapetus ocean water. Geology 26, 1083–1086. https://doi.org/10.1130/0091-
696 7613(1998)026<1083:NICARE>2.3.CO;2
697 Föllmi, K.B., 1996. The phosphorus cycle , phosphogenesis phosphate-rich deposits 40, 55–
698 124. https://doi.org/10.1016/0012-8252(95)00049-6
699 Garnit, H., Bouhlel, S., Jarvis, I., 2017. Geochemistry and depositional environments of
700 Paleocene–Eocene phosphorites: Metlaoui Group, Tunisia. J. African Earth Sci. 134,
701 704–736. https://doi.org/10.1016/j.jafrearsci.2017.07.021
702 Gaškov, M., Sepp, H., Paiste, P., Kirsimäe, K., Pani, T., 2017. Barite mineralization in

703 Kalana speleothems. Est. J. Earth Sci. 66, 12.
704 Girard, C., Lécuyer, C., 2002. Variations in Ce anomalies of conodonts through the
705 Frasnian/Famennian boundary of Poland (Kowala - Holy Cross Mountains):
706 Implications for the redox state of seawater and biodiversity. Palaeogeogr.
707 Palaeoclimatol. Palaeoecol. 181, 299–311. https://doi.org/10.1016/S0031-
708 0182(01)00482-5
709 Goldhammer, T., Brüchert, V., Ferdelman, T.G., Zabel, M., 2010. Microbial sequestration of
710 phosphorus in anoxic upwelling sediments. Nat. Geosci. 3, 557–561.
711 https://doi.org/10.1038/ngeo913
712 Goldstein, S.J., Jacobsen, S.B., 1988. Rare earth elements in river waters. Earth Planet. Sci.
713 Lett. 89, 35–47. https://doi.org/10.1016/0012-821X(88)90031-3
714 Haley, B.A., Klinkhammer, G.P., McManus, J., 2004. Rare earth elements in pore waters of
715 marine sediments. Geochim. Cosmochim. Acta 68, 1265–1279.
716 https://doi.org/10.1016/j.gca.2003.09.012
717 Heinsalu, H., Kaljo, D., Kurvits, T., Viira, V., 2003. The stratotype of the Orasoja member
718 (Tremadocian, Northeast Estonia): Lithology, mineralogy, and biostratigraphy. Proc.
719 Est. Acad. Sci. Geol. 52, 135–154.
720 Heinsalu, H., Viira, V., 1997. Pakerort Stage, in: Raukas, A., Teedumäe, A. (Eds.), Geology
721 and Mineral Resources of Estonia. Estonian Academy Publishers, Tallinn, pp. 331–336.
722 Heinsalu, H., Viira, V., Raudsep, R., 1994. Environmental conditions of shelly phosphorite
723 accumulation in the Rakvere Phosphorite region, Northern Estonia. Proc. Est. Acad. Sci.
724 Geol. 43, 109–121.
725 Herwartz, D., Tütken, T., Jochum, K.P., Sander, P.M., 2013. Rare earth element systematics
726 of fossil bone revealed by LA-ICPMS analysis. Geochim. Cosmochim. Acta 103, 161–
727 183. https://doi.org/10.1016/j.gca.2012.10.038
728 Herwartz, D., Tütken, T., Münker, C., Jochum, K.P., Stoll, B., Sander, P.M., 2011.
729 Timescales and mechanisms of REE and Hf uptake in fossil bones. Geochim.
730 Cosmochim. Acta 75, 82–105. https://doi.org/10.1016/j.gca.2010.09.036
731 Hiller, N., 1993. A modern analogue for the Lower Ordovician Obolus conglomerate of
732 Estonia. Geol. Mag. 130, 265–267. https://doi.org/10.1017/S0016756800009912
733 Jahnke, R.A., 1984. The synthesis and solubility of carbonate fluorapatite. Am. J. Sci. 284,
734 58–78. https://doi.org/10.2475/ajs.284.1.58
735 Jarvis, I., Burnett, W., Nathan, Y., Almbaydin, F., Attia, A.K.M., Castro, L., Flicoteaux, R.,
736 Hilmy, M., Yn, sain V.Q.A.S.A.Z., 1994. Phosphorite geochemistry state-of-the-art and

737 environmental concerns.
738 Jochum, K.P., Wilson, S.A., Abouchami, W., Amini, M., Chmeleff, J., Eisenhauer, A.,
739 Hegner, E., Iaccheri, L.M., Kieffer, B., Krause, J., Mcdonough, W.F., Mertz-Kraus, R.,
740 Raczek, I., Rudnick, R.L., Scholz, D., Steinhoefel, G., Stoll, B., Stracke, A., Tonarini,
741 S., Weis, D., Weis, U., Woodhead, J.D., 2011. GSD-1G and MPI-DING Reference
742 Glasses for In Situ and Bulk Isotopic Determination. Geostand. Geoanalytical Res. 35,
743 Kent, A.J.R., Ungerer, C.A., 2005. Production of barium and light rare earth element oxides
744 during LA-ICP-MS microanalysis. J. Anal. At. Spectrom. 20, 1256–1262.
745 https://doi.org/10.1039/b505734e
746 Kim, J.H., Torres, M.E., Haley, B.A., Kastner, M., Pohlman, J.W., Riedel, M., Lee, Y.J.,
747 2012. The effect of diagenesis and fluid migration on rare earth element distribution in
748 pore fluids of the northern Cascadia accretionary margin. Chem. Geol. 291, 152–165.
749 https://doi.org/10.1016/j.chemgeo.2011.10.010
750 Kocsis, L., Gheerbrant, E., Mouflih, M., Cappetta, H., Ulianov, A., Chiaradia, M., Bardet, N.,
751 2016. Gradual changes in upwelled seawater conditions (redox, pH) from the late
752 Cretaceous through early Paleogene at the northwest coast of Africa: Negative Ce
753 anomaly trend recorded in fossil bio-apatite. Chem. Geol. 421, 44–54.
754 https://doi.org/10.1016/j.chemgeo.2015.12.001
755 Kocsis, L., Osi, A., Vennemann, T., Trueman, C.N., Palmer, M.R., 2009. Geochemical study
756 of vertebrate fossils from the Upper Cretaceous (Santonian) Csehbánya Formation
757 (Hungary): Evidence for a freshwater habitat of mosasaurs and pycnodont fish.
758 Palaeogeogr. Palaeoclimatol. Palaeoecol. 280, 532–542.
759 https://doi.org/10.1016/j.palaeo.2009.07.009
760 Kocsis, L., Trueman, C.N., Palmer, M.R., 2010. Protracted diagenetic alteration of REE
761 contents in fossil bioapatites: Direct evidence from Lu-Hf isotope systematics. Geochim.
762 Cosmochim. Acta 74, 6077–6092. https://doi.org/10.1016/j.gca.2010.08.007
763 Kowal-Linka, M., Jochum, K.P., Surmik, D., 2014. LA-ICP-MS analysis of rare earth
764 elements in marine reptile bones from the Middle Triassic bonebed (Upper Silesia, S
765 Poland): Impact of long-lasting diagenesis, and factors controlling the uptake. Chem.
766 Geol. 363, 213–228. https://doi.org/10.1016/j.chemgeo.2013.10.038
767 Lang, L., Kirsimäe, K., Vahur, S., 2016. Diagenetic fate of bioapatite in linguliform
768 brachiopods: multiple apatite phases in shells of Cambrian lingulate brachiopod Ungula
769 ingrica (Eichwald). Lethaia 49, 13–27. https://doi.org/10.1111/let.12127
770 Lang, L., Puura, I., 2013. Phosphatized organic nanostructures in the Cambrian linguloid

771 brachiopod Ungula inornata (Mickwitz). Est. J. Earth Sci. 62, 121–130.
772 https://doi.org/10.3176/earth.2013.10
773 Lécuyer, C., Grandjean, P., Barrat, J.A., Nolvak, J., Emig, C., Paris, F., Robardet, M., 1998.
774 δ18O and REE contents of phosphatic brachiopods: A comparison between modern and
775 lower Paleozoic populations. Geochim. Cosmochim. Acta 62, 2429–2436.
776 https://doi.org/10.1016/S0016-7037(98)00170-7
777 Lécuyer, C., Reynard, B., Grandjean, P., 2004. Rare earth element evolution of Phanerozoic
778 seawater recorded in biogenic apatites. Chem. Geol. 204, 63–102.
779 https://doi.org/10.1016/j.chemgeo.2003.11.003
780 Lepland, A., Arrhenius, G., Cornell, D., 2002. Apatite in early Archean Isua supracrustal
781 rocks, southern West Greenland: Its origin, association with graphite and potential as a
782 biomarker. Precambrian Res. 118, 221–241. https://doi.org/10.1016/S0301-
783 9268(02)00106-7
784 Lev, S.M., Filer, J.K., 2004. Assessing the impact of black shale processes on REE and the
785 U-Pb isotope system in the southern Appalachian Basin. Chem. Geol. 206, 393–406.
786 https://doi.org/10.1016/j.chemgeo.2003.12.012
787 Lumiste, K., Mänd, K., Bailey, J., Stüeken, E.E., Paiste, K., Lang, L., Sepp, H., Lepland, A.,
788 Kirsimäe, K., 2021. Constraining the conditions of phosphogenesis: Stable isotope and
789 trace element systematics of Recent Namibian phosphatic sediments. Geochim.
790 Cosmochim. Acta 302, 141–159. https://doi.org/10.1016/j.gca.2021.03.022
791 Lumiste, K., Mänd, K., Kirsimäe, K., Bailey, J., Paiste, P., Lang, L., Lepland, A., 2019. REE
792 + Y uptake and diagenesis in Recent sedimentary apatites. Chem. Geol. 525, 268–281.
793 https://doi.org/10.1016/j.chemgeo.2019.07.034
794 Mänd, K., Kirsimäe, K., Lepland, A., Crosby, C.H., Bailey, J. V., Konhauser, K.O., Wirth,
795 R., Schreiber, A., Lumiste, K., 2018. Authigenesis of biomorphic apatite particles from
796 Benguela upwelling zone sediments off Namibia: The role of organic matter in
797 sedimentary apatite nucleation and growth. Geobiology 1–19.
798 https://doi.org/10.1111/gbi.12309
799 Masuda, A., Ikeuchi, Y., 1979. Lanthanide tetrad effect observed in marine environment.
800 Geochem. J. 13, 19–22. https://doi.org/10.2343/geochemj.13.19
801 McArthur, J.M., Walsh, J.N., 1984. Rare-earth geochemistry of phosphorites. Chem. Geol.
802 47, 191–220. https://doi.org/10.1016/0009-2541(84)90126-8
803 McLennan, S.M., 2001. Relationships between the trace element composition of sedimentary
804 rocks and upper continental crust. Geochemistry, Geophys. Geosystems 2, n/a-n/a.

https://doi.org/10.1029/2000GC000109
Minami, M., Masuda, A., Takahashi, K., Adachi, M., Shimizu, H., 1998. Y-Ho fractionation and lanthanide tetrad effect observed in cherts. Geochem. J. 32, 405–419. https://doi.org/10.2343/geochemj.32.405
Munemoto, T., Ohmori, K., Iwatsuki, T., 2015. Rare earth elements (REE) in deep groundwater from granite and fracture-filling calcite in the Tono area, central Japan: Prediction of REE fractionation in paleo- to present-day groundwater. Chem. Geol. 417, 58–67. https://doi.org/10.1016/j.chemgeo.2015.09.024
Neary, M.T., Reid, D.G., Mason, M.J., Friščić, T., Duer, M.J., Cusack, M., 2011. Contrasts between organic participation in apatite biomineralization in brachiopod shell and vertebrate bone identified by nuclear magnetic resonance spectroscopy. J. R. Soc. Interface 8, 282–288. https://doi.org/10.1098/rsif.2010.0238
Nemliher, J., Puura, I., 2001. Apatite varieties in Recent and fossil linguloid brachiopod shells, in: Brunton, H., Cocks, L.R.M., Long, S.L. (Eds.), Brachiopods. CRC Press. https://doi.org/10.1201/9780203210437
Nozaki, Y., Zhang, J., Amakawa, H., 1997. The fractionation between Y and Ho in the marine environment. Earth Planet. Sci. Lett. 148, 329–340. https://doi.org/10.1016/s0012-821x(97)00034-4
Ohr, M., Halliday, A.N., Peacor, D.R., 1994. Mobility and fractionation of rare earth elements in argillaceous sediments: Implications for dating diagenesis and low-grade metamorphism. Geochim. Cosmochim. Acta 58, 289–312. https://doi.org/10.1016/0016-7037(94)90465-0
Ounis, A., Kocsis, L., Chaabani, F., Pfeifer, H.R., 2008. Rare earth elements and stable isotope geochemistry (δ13C and δ18O) of phosphorite deposits in the Gafsa Basin, Tunisia. Palaeogeogr. Palaeoclimatol. Palaeoecol. 268, 1–18. https://doi.org/10.1016/j.palaeo.2008.07.005
Pan, Y., Fleet, M.E., 2002. Compositions of the Apatite-Group Minerals: Substitution Mechanisms and Controlling Factors. Rev. Mineral. Geochemistry 48, 13–49. https://doi.org/10.2138/rmg.2002.48.2
Parrish, J.T., Ziegler, A.M., Scotese, C.R., Humphreville, R.G., Kirschvink, J.L., Cook, P.J., Shergold, J.H., 1986. Phosphate deposits of the World, Volume 1, Proterozoic and Cambrian Phosphorites.
Popov, L.E., Khazanovich, K.K., Borovko, N.G., Sergeeva, S.P., Sobolevskaya, R.F., 1989. The key sections and stratigraphy of the phosphate-bearing Obolus beds on the north-

east of Russian platform. Acad. Sci. USSR, Trans.
Puura, I., 1996. Lingulate brachiopods and biostratigraphy of the Cambrian-Ordovician boundary beds in Baltoscandia. Uppsala University.
Raudsep, R., 1997. Phosphorite, in: Raukas, A., Teedumäe, A. (Eds.), Geology and Mineral Resources of Estonia. Estonian Academy Publishers, Tallinn, pp. 331–336.
Raudsep, R., 1987. Shelly phosphorite: Internal structure of productive seam. Resource characteristics, in: Puura, V. (Ed.), Geology and Mineral Resources of the Rakvere Phosphorite-Bearing Area. Valgus Publishers, pp. 128–142.
Reynard, B., Lécuyer, C., Grandjean, P., 1999. Crystal-chemical controls on rare-earth element concentrations in fossil biogenic apatites and implications for paleoenvironmental reconstructions. Chem. Geol. 155, 233–241. https://doi.org/10.1016/S0009-2541(98)00169-7
Shaw, H.F., Wasserburg, G.J., 1985. Sm-Nd in marine carbonates and phosphates: Implications for Nd isotopes in seawater and crustal ages. Geochim. Cosmochim. Acta 49, 503–518. https://doi.org/10.1016/0016-7037(85)90042-0
Shields, G., Stille, P., 2001. Diagenetic constraints on the use of cerium anomalies as palaeoseawater redox proxies: An isotopic and REE study of Cambrian phosphorites. Chem. Geol. 175, 29–48. https://doi.org/10.1016/S0009-2541(00)00362-4
Shields, G., Webb, G.E., 2004. Has the REE composition of seawater changed over geological time? Chem. Geol. 204, 103–107. https://doi.org/10.1016/j.chemgeo.2003.09.010
Somelar, P., Kirsimäe, K., Hints, R., Kirs, J., 2010. Illitization of early paleozoic k-bentonites in the baltic basin: Decoupling of burial- and fluid-driven processes. Clays Clay Miner. 58, 388–398. https://doi.org/10.1346/CCMN.2010.0580309
Soyol-Erdene, T.O., Huh, Y., 2013. Rare earth element cycling in the pore waters of the Bering Sea Slope (IODP Exp. 323). Chem. Geol. 358, 75–89. https://doi.org/10.1016/j.chemgeo.2013.08.047
Sturesson, U., Popov, L.E., Holmer, L.E., Bassett, M.G., Felitsyn, S., Belyatsky, B., 2005. Neodymium isotopic composition of Cambrian-Ordovician biogenic apatite in the Baltoscandian Basin: Implications for palaeogeographical evolution and patterns of biodiversity. Geol. Mag. 142, 419–439. https://doi.org/10.1017/S0016756805000877
Takahashi, Y., Hayasaka, Y., Morita, K., Kashiwabara, T., Nakada, R., Marcus, M.A., Kato, K., Tanaka, K., Shimizu, H., 2015. Transfer of rare earth elements (REE) from manganese oxides to phosphates during early diagenesis in pelagic sediments inferred

from REE patterns, X-ray absorption spectroscopy, and chemical leaching method. Geochem. J. https://doi.org/10.2343/geochemj.2.0393

Taylor, S.R., McLennan, S.M., 1985. The Continental Crust: Its Composition and Evolution. An Examination of the Geochemical Record Preserved in Sedimentary Rocks. Cont. Crust Its Compos. Evol. An Exam. Geochemical Rec. Preserv. Sediment. Rocks. https://doi.org/10.1017/S0016756800032167

Torsvik, T.H., Van der Voo, R., Preeden, U., Mac Niocaill, C., Steinberger, B., Doubrovine, P. V, van Hinsbergen, D.J.J., Domeier, M., Gaina, C., Tohver, E., Meert, J.G., McCausland, P.J.A., Cocks, L.R.M., 2012. Phanerozoic Polar Wander, Palaeogeography and Dynamics. Earth-Science Rev. https://doi.org/10.1016/j.earscirev.2012.06.007

Tostevin, R., Shields, G.A., Tarbuck, G.M., He, T., Clarkson, M.O., Wood, R.A., 2016. Effective use of cerium anomalies as a redox proxy in carbonate-dominated marine settings. Chem. Geol. 438, 146–162. https://doi.org/10.1016/j.chemgeo.2016.06.027

Trueman, C.N., Kocsis, L., Palmer, M.R., Dewdney, C., 2011. Fractionation of rare earth elements within bone mineral: A natural cation exchange system. Palaeogeogr. Palaeoclimatol. Palaeoecol. 310, 124–132. https://doi.org/10.1016/j.palaeo.2011.01.002

Wallin, B., 1989. Origin of the Lower Cambrian phosphatic bed at Vassbo, Sweden. Terra Nov. 1, 274–279. https://doi.org/10.1111/j.1365-3121.1989.tb00369.x

Webb, G.E.., Nothdurft, L.D., Kamber, B.S., Kloprogge, J.T., Zhao, J.-X., 2009. Rare earth element geochemistry of scleractinian coral skeleton during meteoric diagenesis: a sequence through neomorphism of aragonite to calcite. Sedimentology 56, 1433–1463. https://doi.org/10.1111/j.1365-3091.2008.01041.x

Williams, A., Cusack, M., 2007. Chemico-structural diversity of the Brachiopod shell, in: Selden, P.A. (Ed.), Treatise on Invertebrate Paleontology, Part H, Brachiopoda (Revised). Geological Society of America, Boulder and University of Kansas Press, Lawrence., pp. 2396– 2521.

Williams, A., Cusack, M., 1999. Evolution of a rhythmic lamination in the organophosphatic shells of brachiopods. J. Struct. Biol. 126, 227–240. https://doi.org/10.1006/jsbi.1999.4117

Wright, J., Schrader, H., Holser, W.T., 1987. Paleoredox variations in ancient oceans recorded by rare earth elements in fossil apatite. Geochim. Cosmochim. Acta 51, 631–644. https://doi.org/10.1016/0016-7037(87)90075-5

Zhao, L., Chen, Z.Q., Algeo, T.J., Chen, J., Chen, Y., Tong, J., Gao, S., Zhou, L., Hu, Z., Liu, Y., 2013. Rare-earth element patterns in conodont albid crowns: Evidence for massive

inputs of volcanic ash during the latest Permian biocrisis? Glob. Planet. Change 105, 135–151. https://doi.org/10.1016/j.gloplacha.2012.09.001

Figures

Figure 1. Distribution and thickness of the phosphorite bearing Kallavere Formation and main Estonian phosphorite localities used in this study with corresponding stratigraphic columns. Legend: (1) glauconite sand (2) clay (3) black shale, (4) shelly phosphorite sandstone, (5) siltstone (6) sandstone. Modified after Heinsalu and Viira (1997), Popov et al. (1989), Raudsep (1997, 1987).

Figure 2. Optical and backscattered scanning electron microscope images: (a) complete shells and a phosphatic clast (b) fragmented shells (c) different apatite phases in the phosphorites (Clst –phosphatic clast, Brah. – brachiopod shells. Dia.AP –diagenetic apatite grain coatings.) d) remnant of a brachiopod shell inside a phosphatic clast, e) two distinct apatite laminae present in brachiopod shells (B – mostly authigenic baculate laminae, C – diagenetically altered compact lamina), f) brachiopod shell showing signs of plastic deformation, g) a brachiopod shell intergrown with diagenetic pyrite (Py), h) secondary hematite (Hem) inside a fractured shell. Scale bars represent 100 µm for SEM images, 1000 µm for optical microscopy images.

Figure 3. Backscattered scanning electron (BSE) microscope image (top) of a brachiopod shell and element distribution maps measured by LA-ICP-MS from the area indicated by a dashed line on the BSE image. The concentrations are semi-quantitative. All scale bars are in mg/kg.

Figure 4. Backscattered scanning electron microscope (BSE) image (top) of a phosphatic clast measured by LA-ICP-MS and element distribution maps measured by LA-ICP-MS from the area indicated by a dashed line on the BSE image. The concentrations are semi-quantitative. Ca and P scale bars in counts per second (cps), the rest are mg/kg. **(**Py – pyrite, Brah. – Brachiopod, Clst – phosphatic clast).

Figure 5. PAAS-normalized REE+Y patterns measured from a single (a) *Ungula inornata* and (b) *Ungula ingrica* shell. Both shells from Maardu locality.

Figure 6. Concentrations of (a) ∑REE and (b) U in compact and baculate shell structure types (baculate laminae n = 47, compact laminae n = 29).

Figure 7. PAAS-normalized REE+Y patterns of phosphorite samples from different localities measured by ICP-MS.

Figure 8. Scatter plots of ∑REE and (a) bell-shape index, (b) PAAS-normalized La/Yb ratios, (c) strontium concentrations, (d) MREE/MREE* and HREE/LREE, (e) Y/Ho ratios, (f) Ce-anomalies, (g) PAAS-normalized La/Ce ratios. HREE/LREE ratios is the average of Ho, Er, Tm, Yb, Lu over the average of La, Ce, Pr and Nd. MREE/MREE* is the average of Sm, Eu, Gd, Tb, Dy over the averages of LREE and HREE (*sensu* Haley et al. 2004).

Figure 9. Ce-anomalies in studied samples. Modified after Bau and Dulski (1996). Field I – no La or Ce anomalies. Fields IIa and IIb – apparent negative and positive Ce-anomaly, respectively, Fields IIIa and IIIb – true positive and true negative Ce anomaly, respectively. "Locality LA" denotes laser ablation measurements, "locality" are ICP-MS measurements from a single bulk shell or clast.

Figure 10. Locality-based variations in Y/Ho and Sm_N/Yb_N ratios. Modified after Kocsis et al. (2016) "Locality LA" denotes *in-situ* laser ablation ICP-MS measurements, whereas "locality" are ICP-MS measurements of single bulk shell or clast.

Figure 11. PAAS-normalized REE+Y patterns of phosphatic clasts. The grey areas mark the variability of measured REE+Y values within a locality, the coloured lines mark the REE+Y concentrations of the clast.

Figure 12. Cross-plot of Y-anomalies and PAAS-normalized La/Nd ratios. "Locality LA" denotes *in-situ* laser ablation ICP-MS measurements, whereas "locality" are ICP-MS measurements of single bulk shells or clast. Blue circle marks seawater values *sensu* Shields and Stille (2001).

Figure 13. Cross-plot of PAAS-normalized La/Yb and La/Sm ratios. Modified after Herwartz et al. (2013), data from Deng et al. (2017); Goldstein and Jacobsen (1988); Haley et al. (2004) Kim et al. (2012) and Reynard et al. (1999).

Figure 14. Conceptual model of REE+Y uptake under variable redox conditions. Under reducing conditions, particle-bound REE+Y are released more rapidly, due to the dissolution of carrier phases, driving up pore-water REE+Y concentrations near the SWI. Recrystallization of biogenic apatite likely starts immediately after deposition, allowing more of the REE+Y to be sequestered. Under oxic conditions, initial recrystallization of brachiopod shells occurs in REE+Y depleted pore-water, and the uptake is limited by the availability of these elements. After subsequent burial, more REE+Y are taken up during recrystallization, but still result in lower concentrations.

988

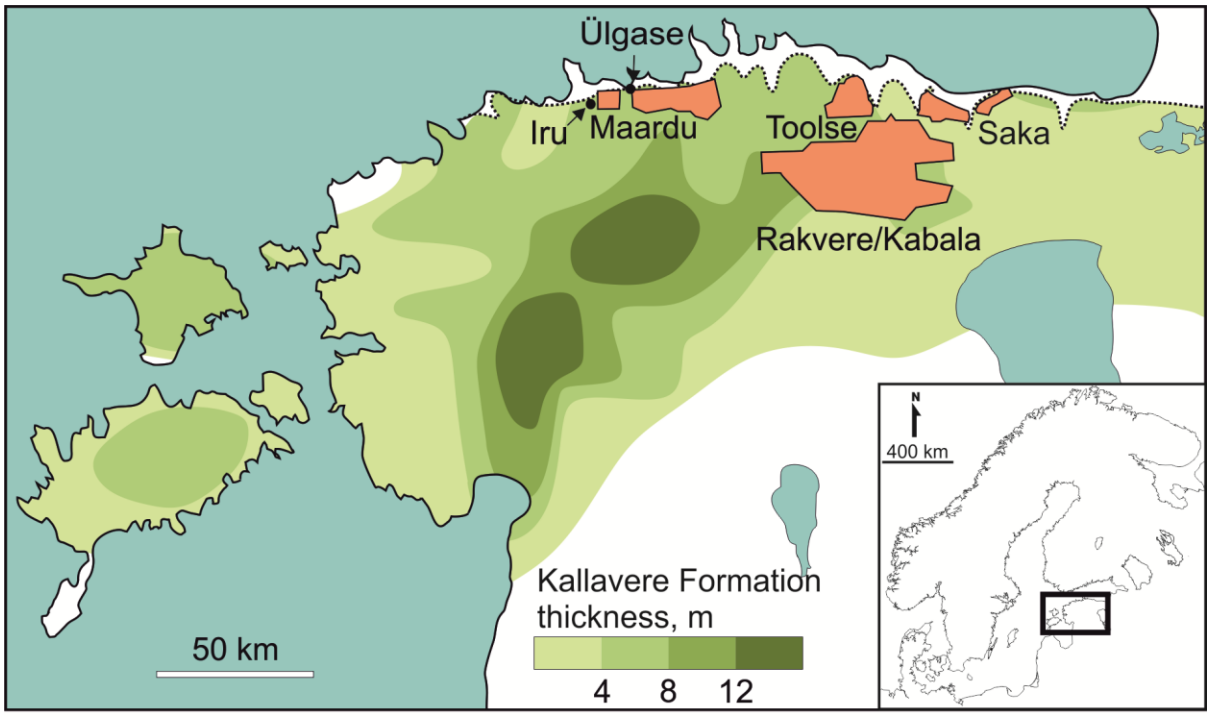
Ülgase
Iru
Maardu
Toolse
Saka
Rakvere/Kabala
50 km
Kallavere Formation
thickness, m
4 8 12
N
400 km

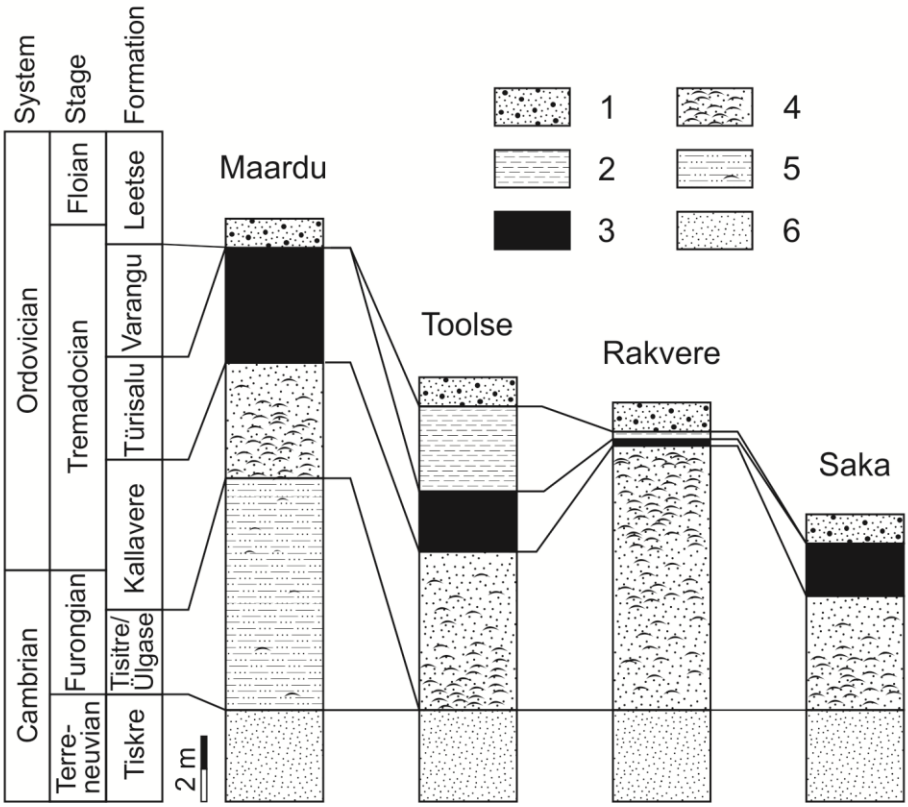
System
Stage
Formation
Ordovician
Cambrian
Floian
Tremadocian
Furongian
Terre-neuvian
Leetse
Varangu
Türisalu
Kallavere
Tisitre/ Ülgase
Tiskre
2 m
Maardu
Toolse
Rakvere
Saka
1
2
3
4
5
6

989

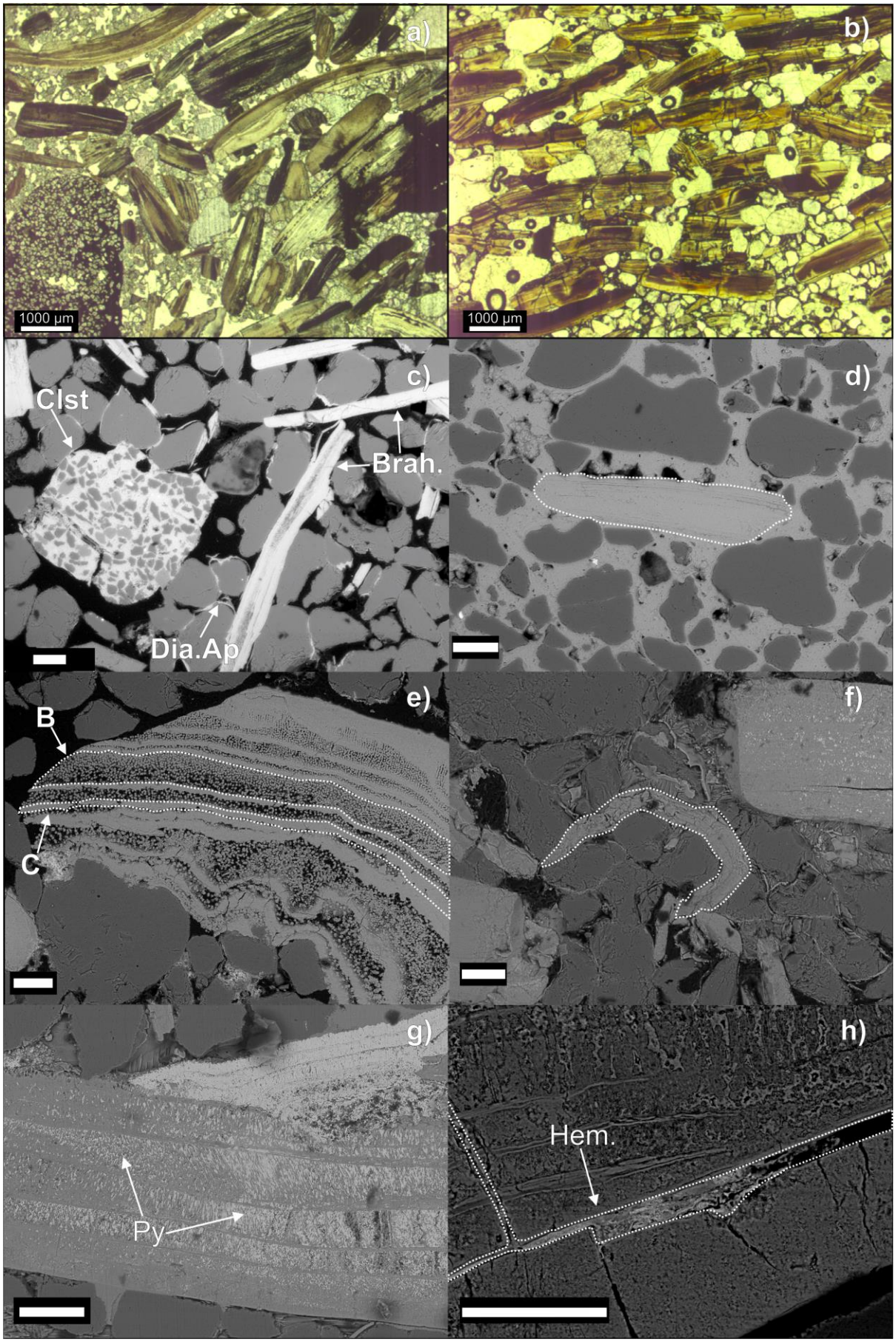

990

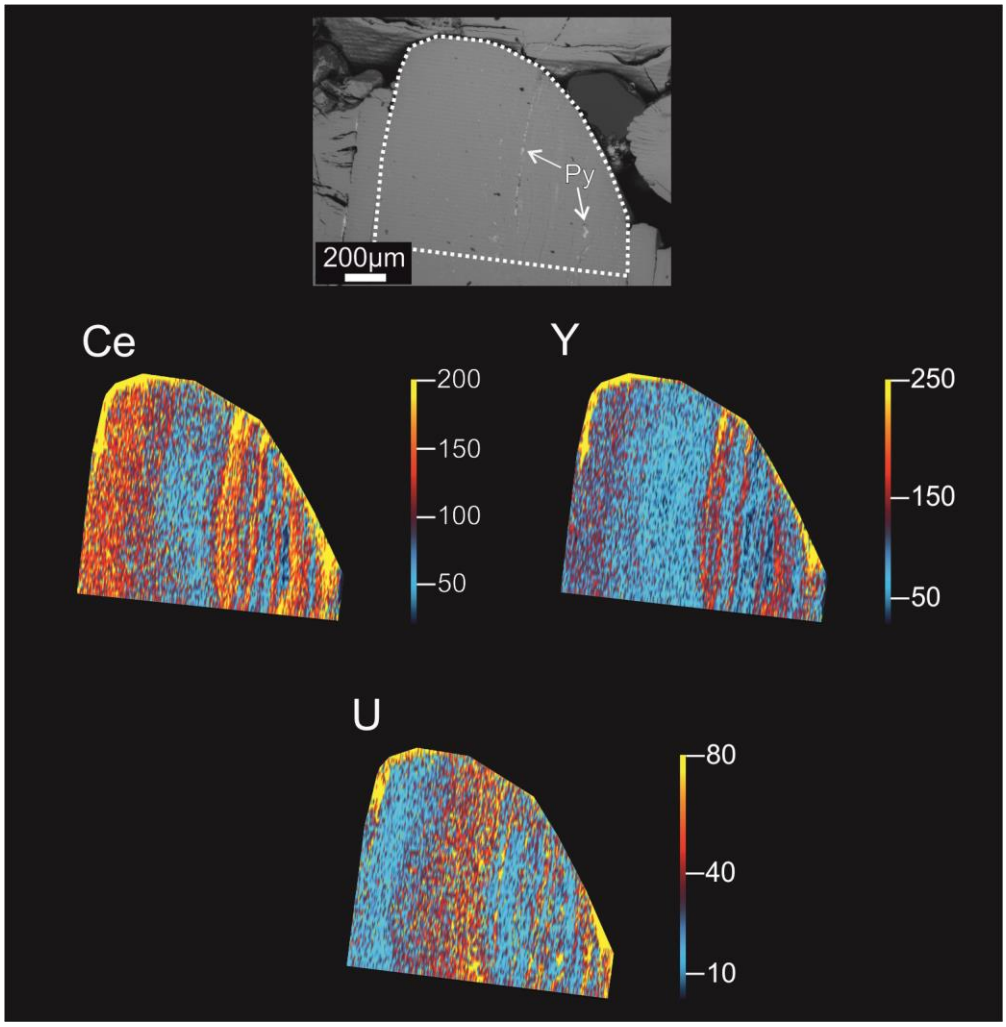

991

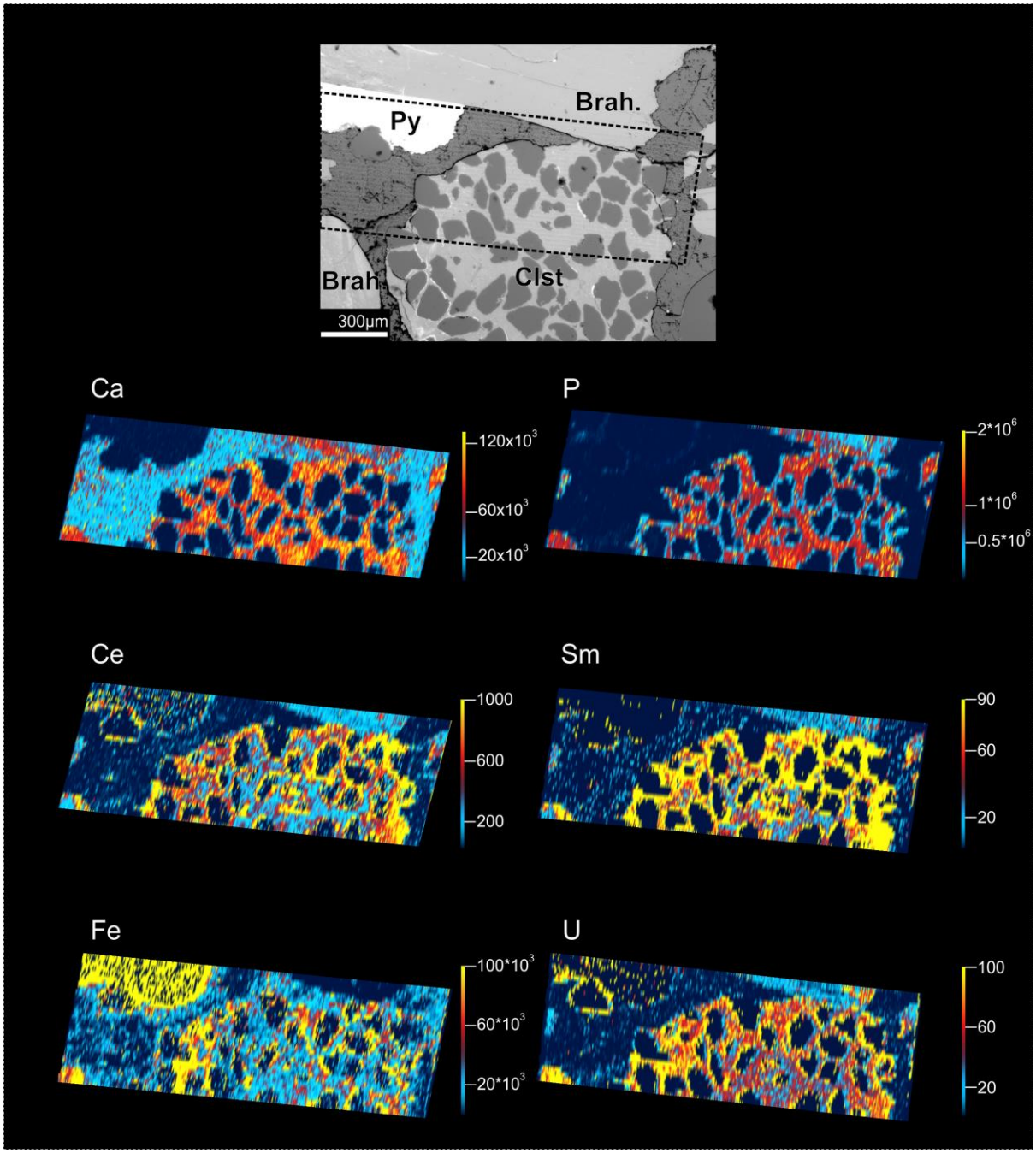
Py
Brah.
Brah
Clst
300µm
Ca
120x10^3
60x10^3
20x10^3
P
2*10^6
1*10^6
0.5*10^6
Ce
1000
600
200
Sm
90
60
20
Fe
100*10^3
60*10^3
20*10^3
U
100
60
20

992

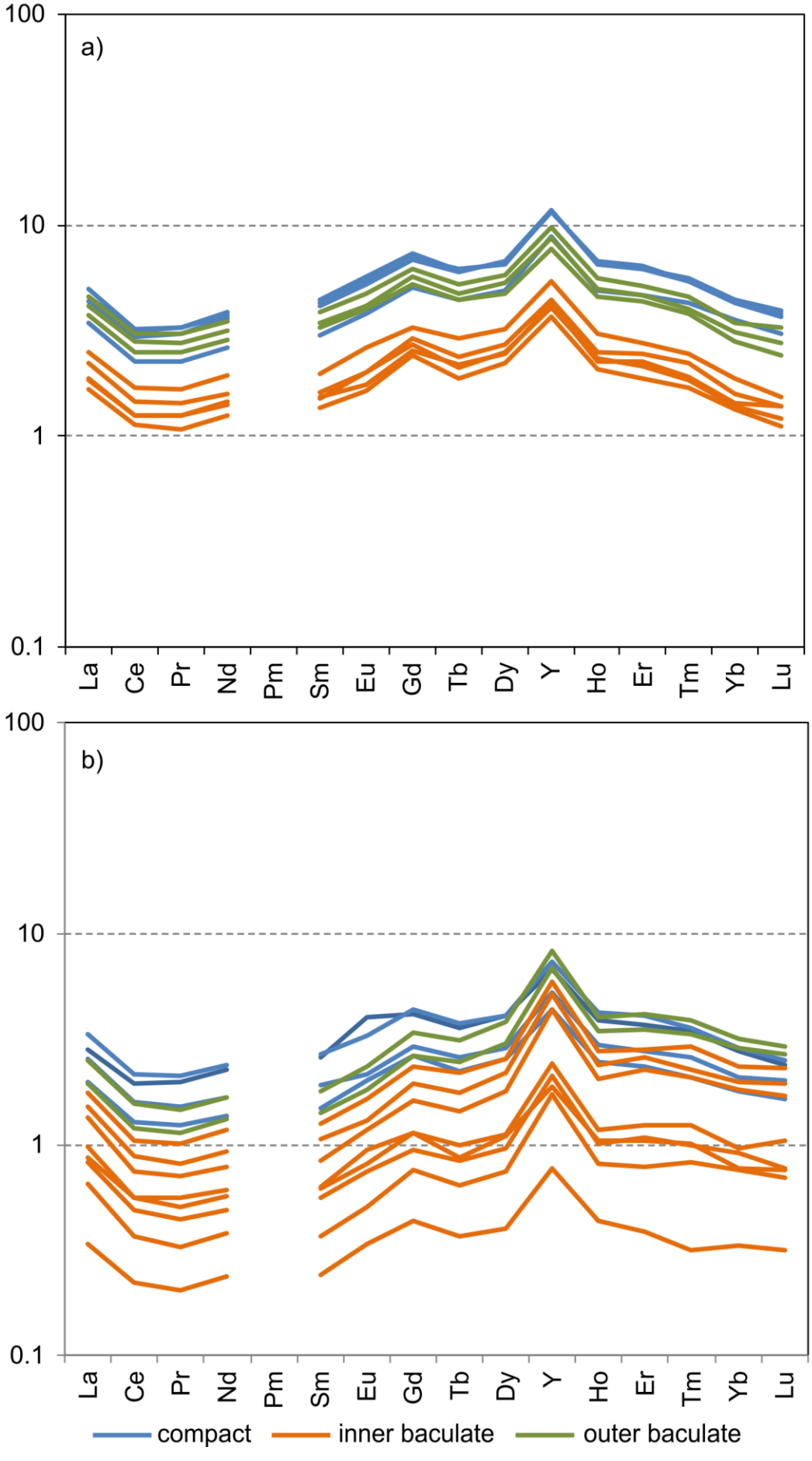
a)
b)
100
10
1
0.1
La
Ce
Pr
Nd
Pm
Sm
Eu
Gd
Tb
Dy
Y
Ho
Er
Tm
Yb
Lu
compact
inner baculate
outer baculate

993

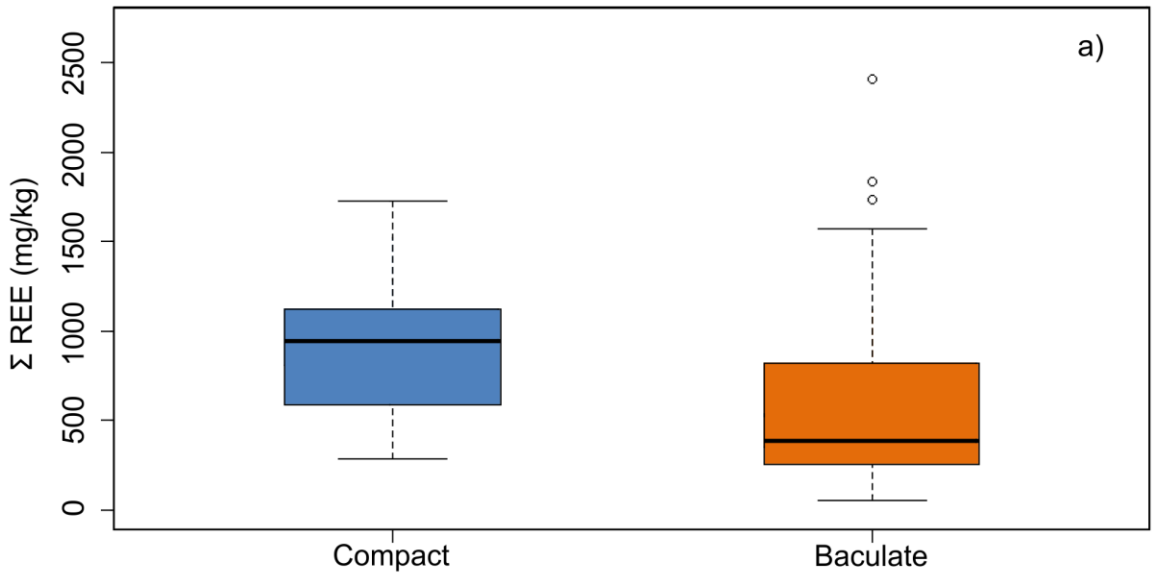
a)
Σ REE (mg/kg)
0
500
1000
1500
2000
2500
Compact
Baculate

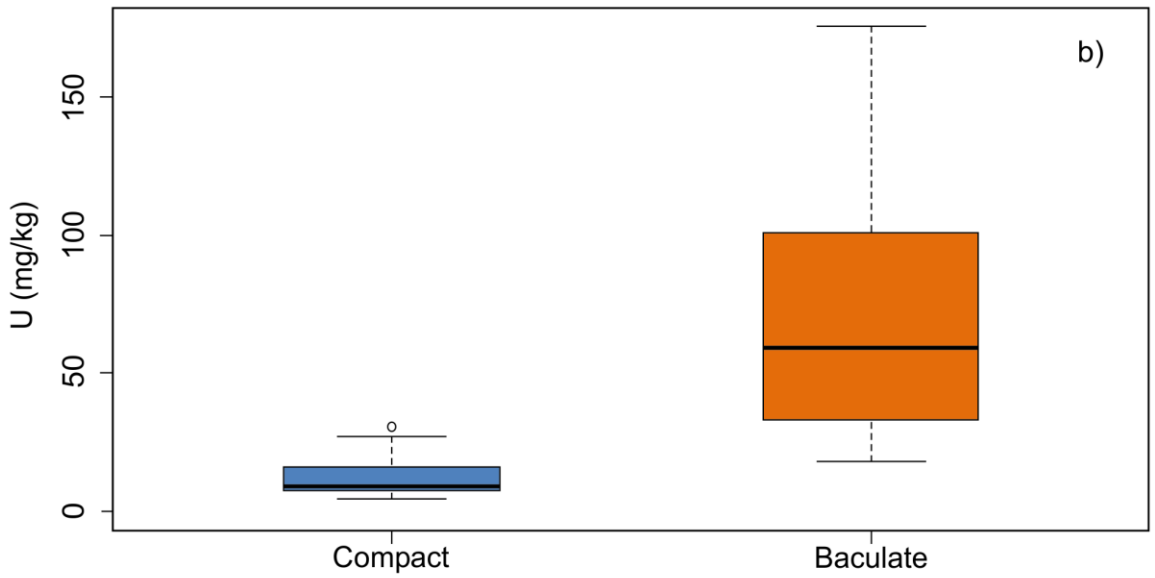
b)
U (mg/kg)
0
50
100
150
Compact
Baculate

994

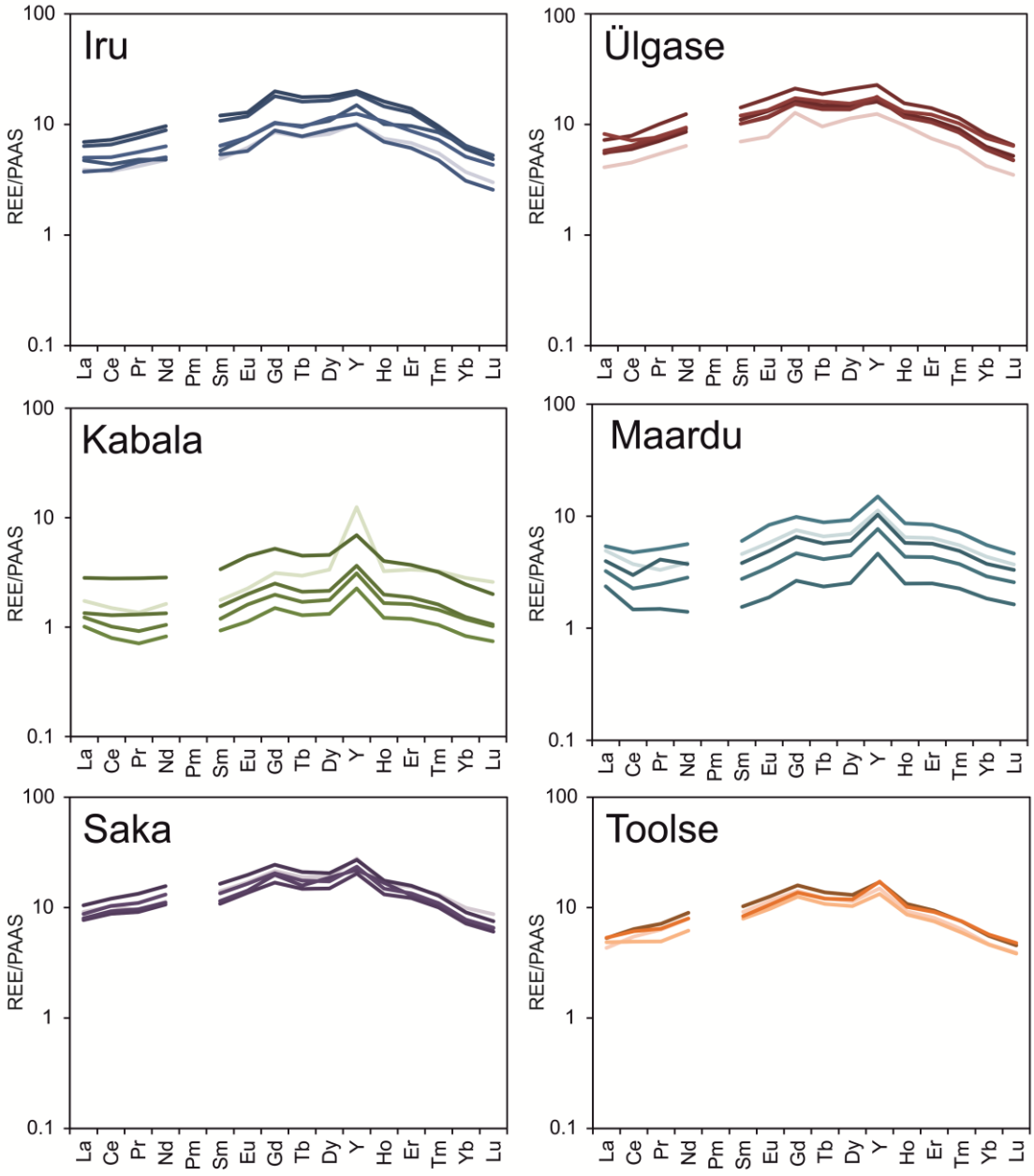
Iru
Ülgase
Kabala
Maardu
Saka
Toolse
REE/PAAS
100
10
1
0.1
La
Ce
Pr
Nd
Pm
Sm
Eu
Gd
Tb
Dy
Y
Ho
Er
Tm
Yb
Lu

995

996

997

998

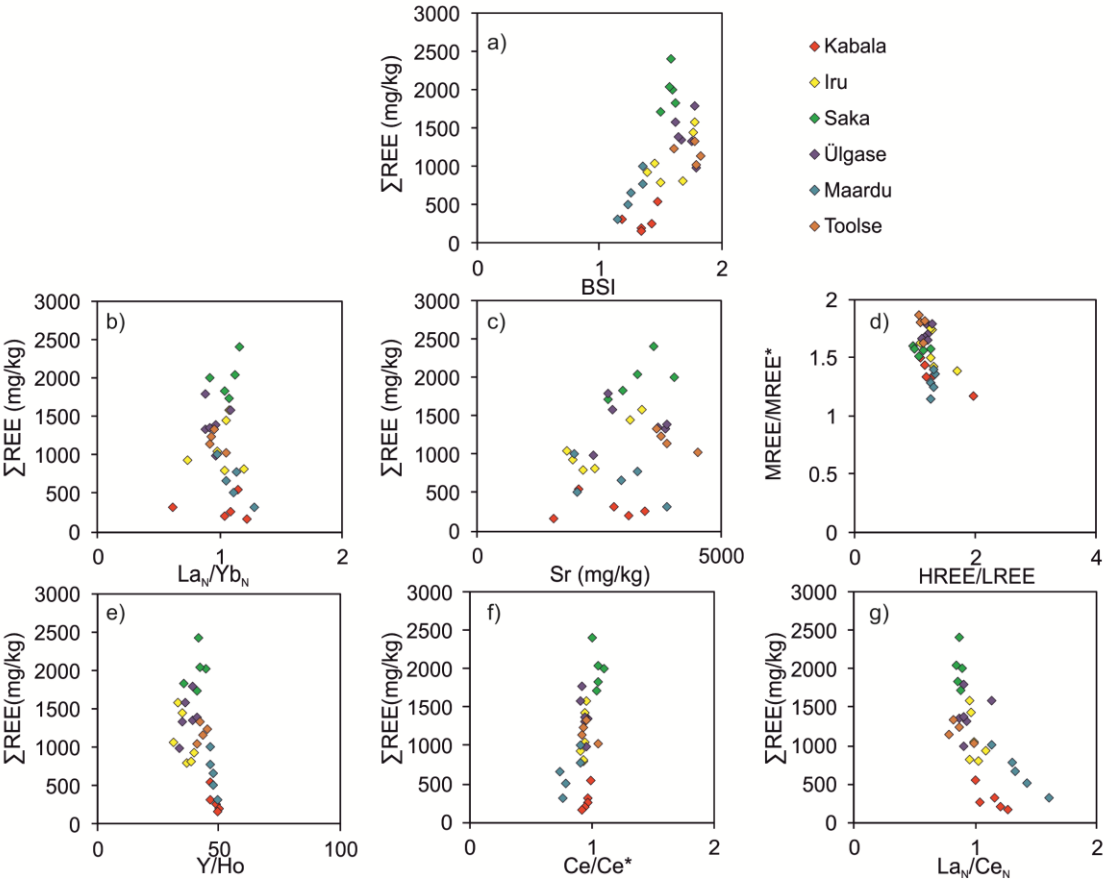
a)
ΣREE (mg/kg)
BSI
Kabala
Iru
Saka
Ülgase
Maardu
Toolse
b)
ΣREE (mg/kg)
La$_N$/Yb$_N$
c)
ΣREE (mg/kg)
Sr (mg/kg)
d)
MREE/MREE*
HREE/LREE
e)
ΣREE(mg/kg)
Y/Ho
f)
ΣREE(mg/kg)
Ce/Ce*
g)
ΣREE(mg/kg)
La$_N$/Ce$_N$

999

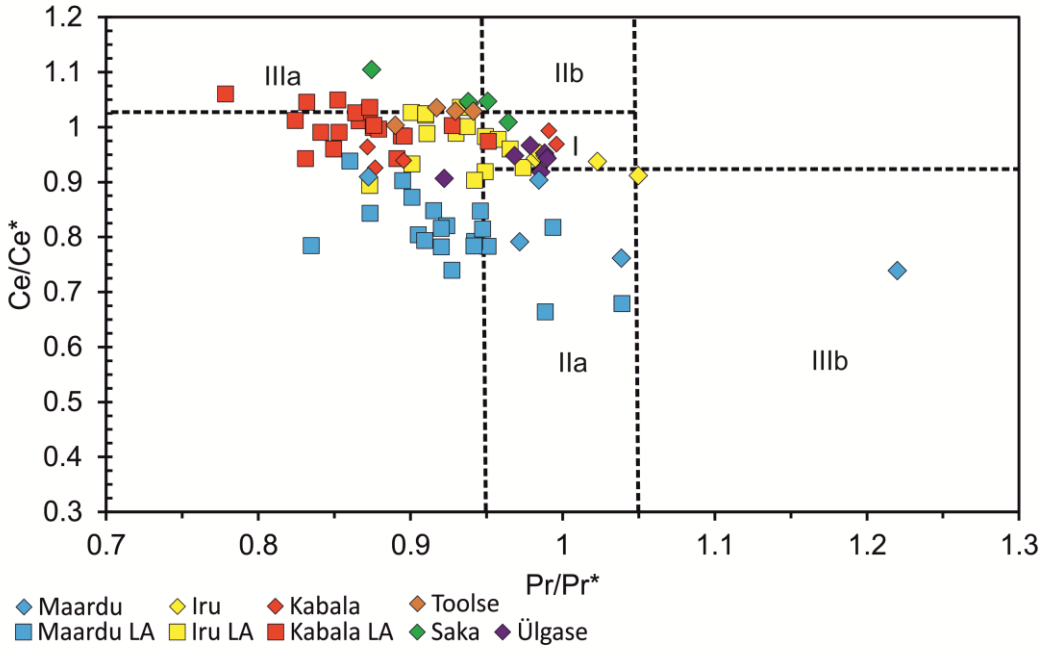
IIIa
IIb
I
IIa
IIIb
Ce/Ce*
Pr/Pr*
Maardu
Iru
Kabala
Toolse
Maardu LA
Iru LA
Kabala LA
Saka
Ülgase

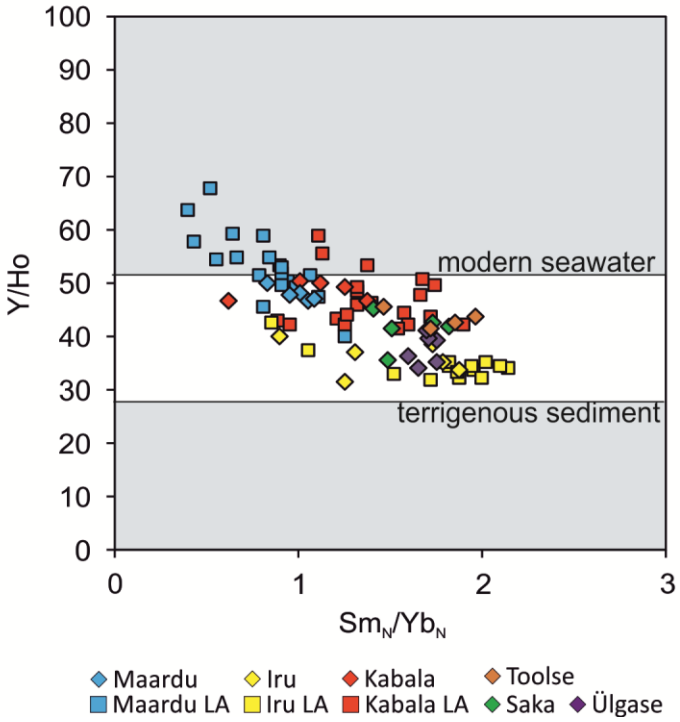
100
90
80
70
60
50
40
30
20
10
0
Y/Ho
modern seawater
terrigenous sediment
0
1
2
3
Sm_N/Yb_N
Maardu
Maardu LA
Iru
Iru LA
Kabala
Kabala LA
Toolse
Saka
Ülgase

1000

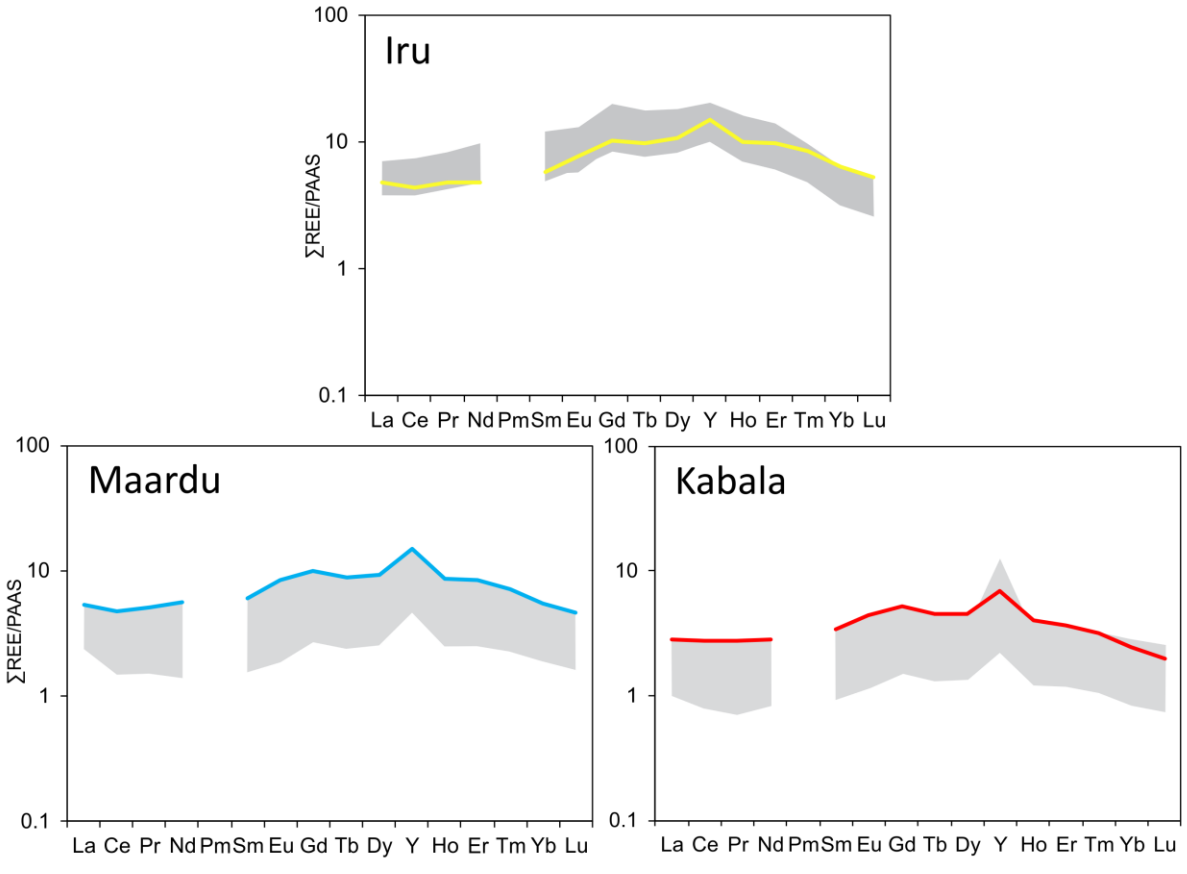
Iru
Maardu
Kabala
100
10
1
0.1
∑REE/PAAS
La Ce Pr Nd Pm Sm Eu Gd Tb Dy Y Ho Er Tm Yb Lu

1001

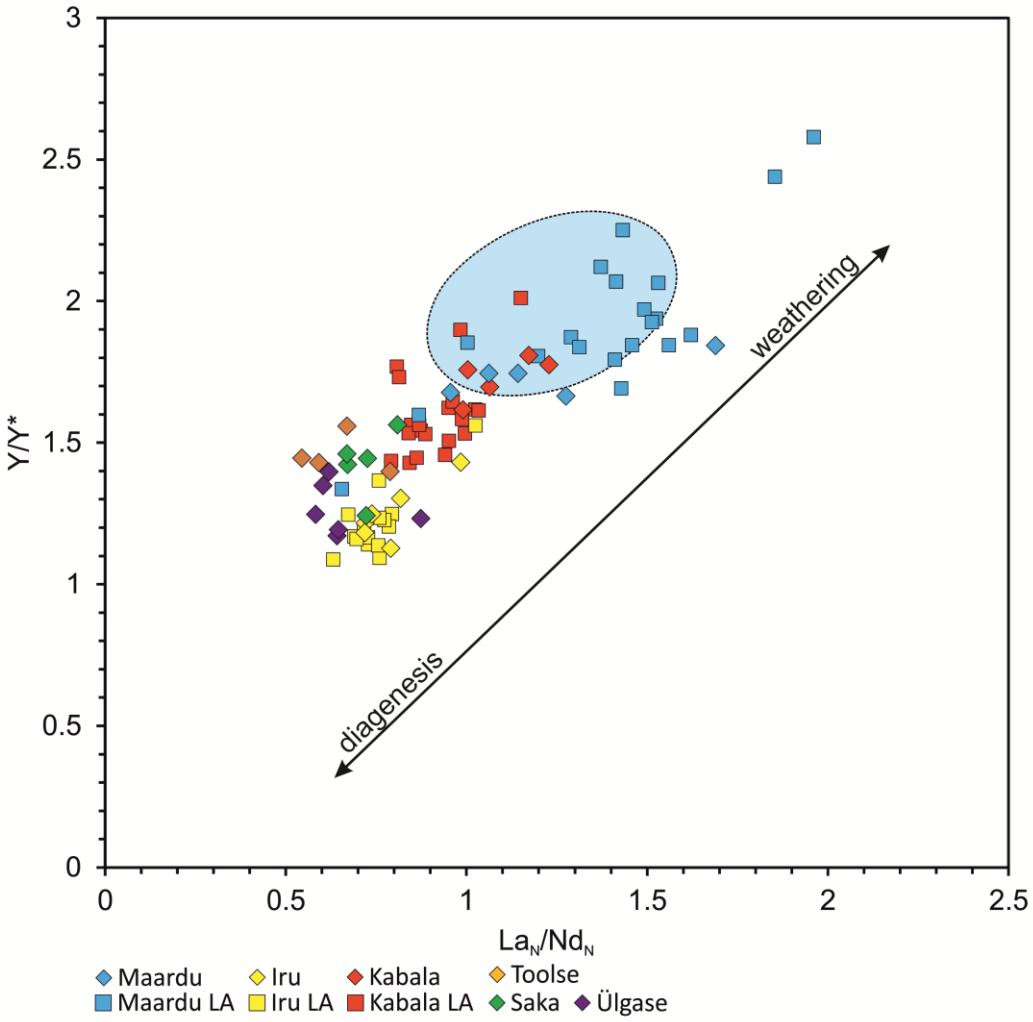
3
2.5
2
1.5
1
0.5
0
Y/Y*
0
0.5
1
1.5
2
2.5
La$_N$/Nd$_N$
weathering
diagenesis
Maardu
Maardu LA
Iru
Iru LA
Kabala
Kabala LA
Toolse
Saka
Ülgase

1002

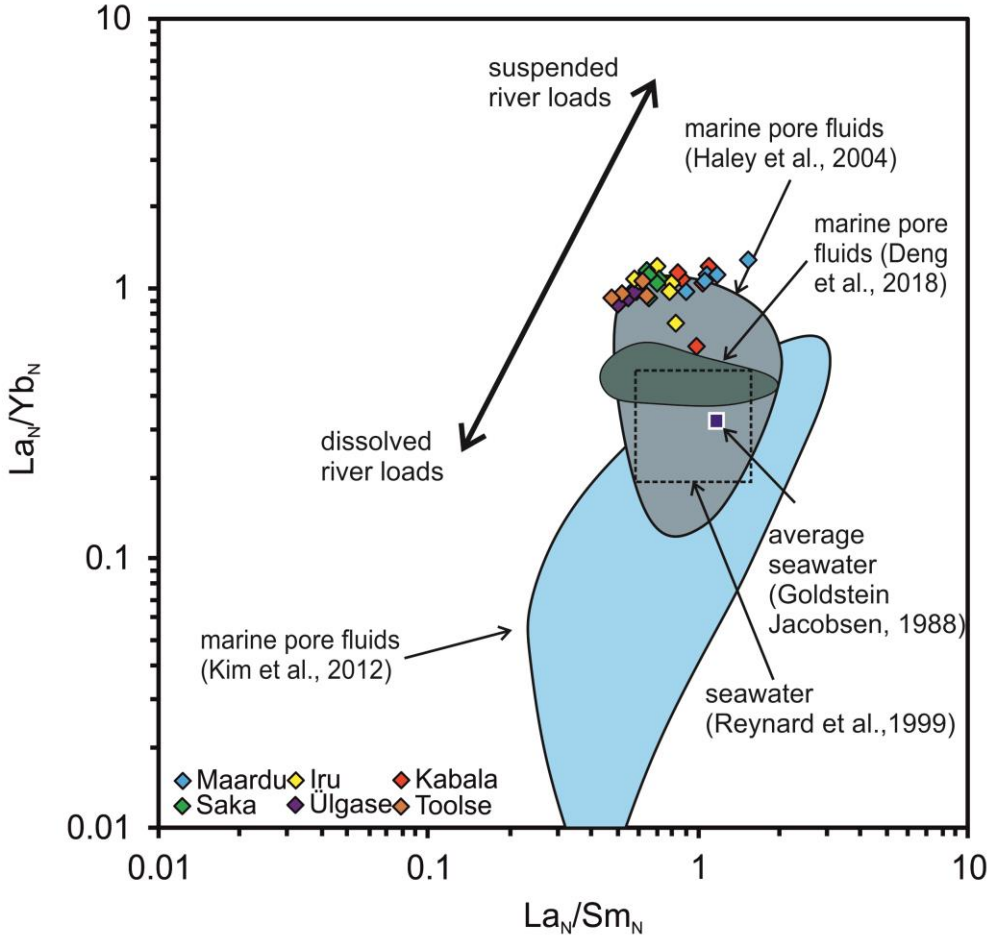
10
1
0.1
0.01
0.01
0.1
1
10
La$_N$/Yb$_N$
La$_N$/Sm$_N$
suspended
river loads
marine pore fluids
(Haley et al., 2004)
marine pore
fluids (Deng
et al., 2018)
dissolved
river loads
average
seawater
(Goldstein
Jacobsen, 1988)
marine pore fluids
(Kim et al., 2012)
seawater
(Reynard et al.,1999)
Maardu
Iru
Kabala
Saka
Ülgase
Toolse

1003

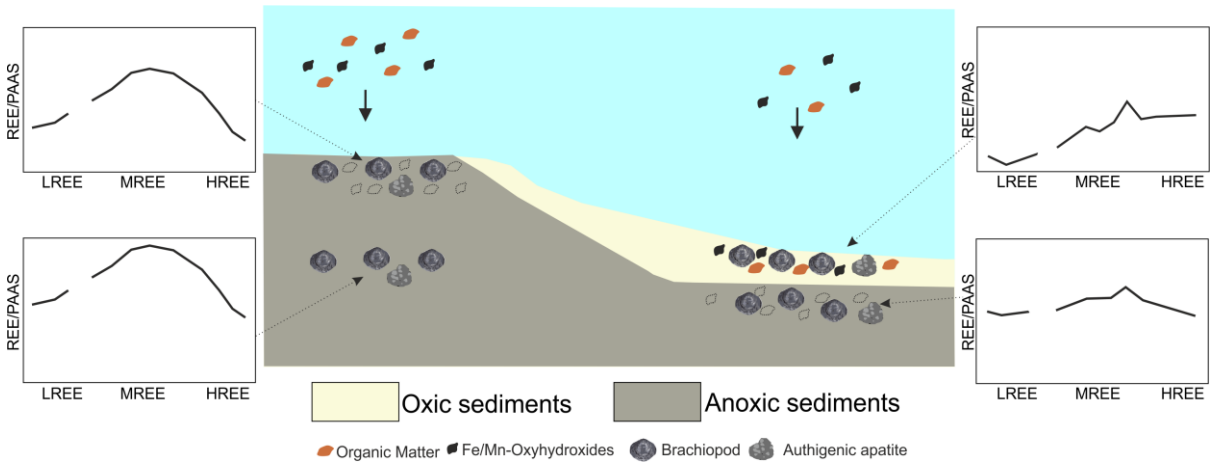
REE/PAAS
LREE
MREE
HREE
Oxic sediments
Anoxic sediments
Organic Matter
Fe/Mn-Oxyhydroxides
Brachiopod
Authigenic apatite

1004